Dual linker UNC-10/SYD-2 is sufficient to bind kinesin-3 UNC-104 to RAB-3 containing synaptic vesicles in the absence of the motor's PH domain

Prerana Bhan, Odvogmed Bayansan, Chien-Yu Chang and Oliver Ingvar Wagner*

National Tsing Hua University, Institute of Molecular and Cellular Biology, Department of Life Science, Hsinchu, 30013, Taiwan (R.O.C.)

Running title: The effect of RAB-3-UNC-10-SYD-2 complex on UNC-104.

***Corresponding author**:

Dr. Oliver I. Wagner

Professor

National Tsing Hua University

Institute of Molecular and Cellular Biology & Department of Life Science

101, Sec. 2, Kuang-Fu Road, Hsinchu 30013, Taiwan (R. O. C.)

Email: owagner@life.nthu.edu.tw

Phone: +886-3-574-2487, Fax: +886-3-571-5934

Keywords: SYD-2, UNC-10, RAB-3, kinesin-3, SNB-1, UNC-104.

Conflicts of interest: The authors declare no conflict of interest.

Abstract

KIF1A (UNC-104 in *C. elegans*) is the major fast axonal transporter of synaptic vesicles and heritable mutations in neuronal motor proteins (and their adaptors) lead to numerous neurodegenerative diseases. The C-terminal PH domain of UNC-104 specifically and directly binds to phosphatidylinositol 4,5-bisphosphate in membranes of STVs (synaptic vesicle protein transport vesicles). Based on literature evidences, we hypothesize that RAB-3-bound STVs may employ a dual linker UNC-10/SYD-2 to connect to UNC-104. This RAB-3/UNC-10/SYD-2 linker may act as an additional reinforcement for the (supposed) weak motor-lipid interaction. As a first approach, we provide genetic evidence for such a tripartite linker system since syd-2 gene expression increased in *unc-10* mutants, while in *rab-3* mutants it decreased. These findings are consistent with Western blot analysis in these mutants using anti-SYD-2 antibodies. Co-immunoprecipitation assays revealed reduced SYD-2/UNC-104 binding in both *unc-10* and *rab-3* mutants. SYD-2/UNC-104 colocalization as well as bimolecular fluorescence complementation assay (BiFC) signals were also diminished in both *unc-10* and *rab-3* mutants. In sublateral and ALM neurons of these mutants, UNC-104 appears to be more diffused and is unable to travel longer distances with visibly reduced speeds. Critically, the dual SYD-2/UNC-10 linker seems to be critical for RAB-3-containing vesicles but not for SNB-1-containing vesicles, pointing to the specificity of our proposed model. Moreover, deletion of the motor's PH domain did not affect UNC-104/RAB-3 colocalization, while it did affect UNC-104/SNB-1 colocalization. These findings supporting the idea of a dual UNC-10/SYD-2 linker acting as an sufficient buttress to connect the motor to RAB-3-containing vesicles.

Introduction

The active transport of organelles and proteins is becoming an exciting frontier of neuroscience. The neuronal cytoskeleton is primarily composed of microtubules (MTs), actin filaments and neurofilaments (NFs) that function in the establishment and maintenance of neuronal polarity, morphology and integrity of axons [1-3]. The MT dynamics is regulated by a large number of factors such as, microtubule associated proteins (MAPs), motor proteins, and post-translational tubulin modifications [4-7]. Axonal transport supplies axons and nerve terminals with proteins, lipids and mitochondria and prevents the build-up of misfolded proteins and toxic aggregates [8]. Due to the unique microtubule polarity, Kinesins play a pivotal role in the anterograde transport (from cell body to synapse) of axonal proteins while dynein is required for the retrograde transport that aids in recycling the components from the synapse back to the cell body [9]. In recent years, axonal transport has gained much importance due to its association with several neurological diseases. Neurodegenerative diseases are caused due to defects in axonal transport, its outgrowth, targeting of proteins and synapse functioning [10-12].

KIF1A is a neuron specific molecular motor belonging to the kinesin-3 family and is termed as UNC-104 in *C.elegans.* UNC-104 is a transporter of synaptic vesicle precursors such as RAB-3, synaptotagmin, synaptobrevin and synaptophysin in axons [13 14]. In another study, it has been shown that IDA-1 in *unc-104* mutants revealed that UNC-104 kinesin is also a major transporter of dense core vesicles (DCVs) in axons [15]. KIF1A deficient-mice resulted in neuronal degeneration and cell death, thereby playing an essential role in maintenance and viability of neurons [16]. Moreover in *C.elegans,* synaptic vesicles misaccumulate in the neuronal cell bodies leading to worm paralysis, indicating defects in axonal transport [13]. It is also been shown previously that UNC-104 is required for dendrite morphogenesis and synaptic development in

Drosophila [17]. Further, *unc-104* mutants' exhibits structural defects in the formation of active zone at the neuromuscular junctions providing evidence for the importance of UNC-104 in site-specific synapse maturation [18]. Mutations in KIF1A/UNC-104 leading to defects in axonal transport are often the major cause of neurological disorders like Marie Charcot tooth disease, amyotrophic lateral sclerosis etc. [19 20]. In *C.elegans*, KIF1A/UNC-104 associates with Tau/PTL-1 and affects the transport behavior of the motor [21]. KIF1A motors are inactive or undergo slow processive movements in monomeric state. However, they dimerize utilizing their coil-coiled domains and form active homodimers that are super-processive in nature [22]. More interestingly, the PH domain of UNC-104 specifically binds to phosphatidylinositol-4, 5-bisphosphate [(PI(4,5)P_2)] facilitating UNC-104-mediated axonal transport [23].

The active zone is evolutionarily conserved and morphologically defined as the site of synaptic vesicle cluster, docking, fusion and release [24]. Over the past decades, a wide variety of proteins that associate with the mammalian active zone have been identified [for reviews: [25-28]. The active zone proteins identified in *C.elegans* so far are UNC13, Rab-3, UNC-10, SYD-2, LIN-2, CLA-1 respectively. The link between synaptic vesicle trafficking and active-zone components are not well understood. Although, in several recent studies the relationship between UNC-104/SYD-2 [29], UNC-104/RAB-3 [30], UNC-104/CLA-1[31] and UNC-104/LIN-2 [32] have provided key insights into the trafficking mechanism. However, future studies are necessary to understand how the molecular motor regulated axonal transport ensures targeting of appropriate proteins to the presynaptic active zone.

Syd-2 is a multi-domain scaffolding protein that shows structural homology to the vertebrate presynaptic protein Liprin-α [33-35]. SYD-2 comprises of N-terminal coiled coils and three alpha-sterile motifs (SAM domains) that interacts with each other and inactivates the protein via

intramolecular folding mechanism [36]. *Syd-2 loss of function* mutants causes active zones to become less compact, more elongated with smaller dense projection thereby causing impairment of synaptic vesicle docking and synaptic transmission [33 37 38]. Consistent with these findings, SYD-2's N' terminal domain has been found to directly associate and colocalize with other synaptic proteins such as CAST/ELKS, GIT1 and UNC-10/RIM [39-43]. Furthermore, SYD-2's SAM domain interacts with UNC-104's FHA domain and that this association results in motor protein activation and enhanced clustering [29]. In another study, akin to UNC-104's role in transporting dense core vesicles containing neuropeptides, SYD-2 also regulates the mobility and distribution of dense-core vesicles [44]. Moreover, similar to the interaction with UNC-10, SYD-2/RAB-3 binding is also required to maintain synaptic vesicle's at the dense projection [45]. SYD-2 and UNC-104 also have dual roles in maintaining synaptic vesicle cluster stability and transport [46].

RIMs are a family of multi-domain scaffolding proteins that were initially identified as putative Rab3 effectors that regulates synaptic vesicle fusion [47]. RIM homolog identified in nematode *C.elegans* is UNC-10 [48] that is composed of N-terminal zinc finger motif, a central PDZ domain, two C-terminal C2 domains (C2A and C2B) and a short proline-rich SH3 motif respectively [49]. RIM/UNC-10 interacts with multiple synaptic proteins mainly the N-terminal zinc finger interacts with GTP bound Rab3 [47] and C2B domains associate with the N-terminal of SYD-2/liprin-α [50]. The dynamics of RIM and CASK are closely monitored by Liprin-α, it regulates presynaptic organization by anchoring active zone (AZ) proteins RIM1 and CASK to facilitate synaptic vesicle (SV) release [41]. Consequently, RIM1α is also required for maintaining the presynaptic long-term potentiation [51]. Furthermore, Christian et al. have shown that UNC-10 and SYD-2 act in the same pathway to regulate synaptic vesicles [37]. Although, no direct evidence is available for

the role of UNC-10 in regulating UNC-104, therefore one may speculate its role via the regulation of SYD-2 and RAB-3 by the formation of a tripartite complex or by the regulation of dense core vesicles that are known to be docked and primed by UNC-10 for its exocytosis.

Rab3/RAB-3 is a member of RAB family of small GTPases that recruits synaptic vesicles for exocytosis [52]. Rab3A attaches to the synaptic vesicles via the C-terminal and the carboxy terminal sequence Cys-X-Cys is highly conserved in invertebrates [53]. Rab-3A binds to synaptic vesicles in their GTP-bound state and dissociation occurs due to GTP-hydrolysis [54]. In addition, Rab3A null mutant mice [52] and worms [30] display mild phenotypes. However, *C.elegans rab3* null mutants have fewer synaptic vesicles near the active zone indicating impaired synaptic vesicle transport in the absence of *rab3* [30]. While most of the studies in rab3 focus on synaptic vesicle transport, it is also noteworthy to know that rab3 regulates the localization of many presynaptic proteins to active zones [55]. Concomitantly, the proper localization of presynaptic proteins stimulate synaptic transmission and neurotransmitter release via rab3 exchange factor homologue, AEX-3 [56 57]. Rab3A is transported to the active zone by the fast anterograde axonal transport system in axons [58]. A recent study suggested that KIF1A associates to rab3 carrying vesicles via the linker DENN/MADD [59], the homolog of which is identified as AEX-3. Another synaptic vesicle precursor SNB-1::GFP was found to express in the nervous system of *C.elegans* and antibody staining displayed colocalization with synaptotagmin [60]. In *unc-104* mutants, SNB-1 mislocalized in the neuronal cell bodies [61]. Mutants lacking *snb-1* are embryonically lethal, therefore SNB-1 is essential for viability and synaptic transmission [61].

Previous studies have suggested that the binding of PH domain to lipid surface is weak and non-specific [62] therefore we propose that this association may be insufficient and that an additional linker is required to support the motor-cargo association and connectivity. Especially, regarding

the notion that the cargo/vesicle is of multiple size of the motor, the transport has to overcome the strong viscous drag in the crowded axoplasm. In this study, we propose an existence of an additional linker that connects the motor to its cargo. Based on this knowledge, we hypothesize the following interaction chain: "UNC-104 (KIF1A) = SYD-2(Liprin-α) = UNC-10(RIM) = RAB-3(RAB3) = vesicle". In the present study, using molecular and cell biological approaches, we provide evidences on how UNC-10/RAB-3 complex enhances the binding of SYD-2 to UNC-104. Further, we also provide evidence to show that this tripartite complex (linker) acts as an adaptor for UNC-104 to selectively transport RAB-3 containing vesicles.

Results

Relative expression of syd-2 in *unc-10* and *rab-3* mutants

To investigate if our proposed model can be applied to UNC-104-based axonal transport, we first sought to understand the relative expression of *syd-2* in *unc-10* and *rab-3* mutant backgrounds respectively. Because in our model, we propose the presence of an additional linker, it is important to understand the relationship between SYD-2/UNC-10/RAB-3. The UNC-104/SYD-2 interaction has been well-described [29 36] also UNC-104, SYD-2 and UNC-10 are associated with dense core vesicle trafficking [15 44], therefore the proof of a physical interaction between SYD-2, UNC-10 and RAB-3 would also help to understand the tripartite phenomena. As a result, monitoring the expression level of *syd-2* in adult worms, we found that *syd-2* expression level increases in *unc-10(md1117)* and *unc-10(e102)* allelic mutant backgrounds by two fold (Figure 1A), while its expression is reduced by 50% in *rab-3(js49)* mutants (Figure 1B). *Syd-2* expression was normalized to endogenous *cdc-42* as internal control.

Functional interaction between SYD-2 and UNC-104 in *unc-10* and *rab-3* mutants

The above result encouraged us to understand if the proposed linker aids in enhancing the interaction of the motor to its cargo. At first we need to understand whether UNC-10 and RAB-3 play a role in the UNC-104/SYD-2 complex. Therefore, we set out to understand if UNC-10 and RAB-3 would affect the binding of SYD-2 to UNC-104. Indeed, precipitating UNC-104::GFP (using anti-GFP antibodies) from whole worm lysates, we found that SYD-2 levels were reduced in the *unc-10(md1117)* knockout mutant (Figure 1E+F), whereas in lysates from worms carrying *unc-10* point mutations (*e102* allele; point mutation in the C_2A domain resulting in a weak coiler phenotype; Figure 1E+F), SYD-2 levels were mildly reduced (for antibody details, please refer to the Methods and Materials section). The qPCR analysis from Figure 1A is also comparable to the Western blot bands in Figure 1E lysate section quantified in Figure 1C, careful observation indicates that the relative expression level of *syd-2* is elevated in *e102* and *md1117* mutants. In addition, %SYD-2 signal intensity from the IP blots were also quantified that exhibits the reduction of SYD-2 expression in *unc-10* mutants (Figure 1F) further suggesting that the absence of UNC-10 robustly affects the interaction of SYD-2 with UNC-104.

Likewise, when precipitating UNC-104::mRFP from whole worm lysates, we found that SYD-2 expression levels were significantly reduced in *js49* mutants (Figure 1G+H). Also, the qPCR analysis quantifying the relative expression of SYD-2 in *rab-3(js49)* mutant is comparable to the Western blot bands indicating a reduction in *syd-2* relative expression (Compare lysate section Figure 1G quantified in Figure 1D with Figure 1B). Furthermore, the %SYD-2 signal intensity quantified from the IP blots (Figure 1H) further confirms that the absence of RAB-3 affects SYD-2's binding to UNC-104.

Finally, these data validates our hypothesis that UNC-104/SYD-2 interactions indeed require UNC-10 and RAB-3 to strengthen its association.

SYD-2 and UNC-104 interaction is dependent on UNC-10 and RAB-3

Active zone proteins SYD-2, UNC-10 and RAB-3 colocalize with each other and are also co-transported in *C.elegans* DA9 motor neurons [45]. In another study, it has also been shown that SYD-2 colocalizes with UNC-104 [29]. Although, raising questions of how SYD-2/UNC-104 colocalization can be regulated by UNC-10 and RAB-3. To address this question, we investigated the colocalization of UNC-104 and SYD-2 in the absence of UNC-10 and RAB-3 in the nerve ring of living nematodes. It is evident from our data that in wild-type animals UNC-104 and SYD-2 display a high degree of colocalization (Figure 2A+B). However, colocalization is significantly affected in the absence of both UNC-10 and RAB-3. This further implicates the presence of an additional linker that is required to facilitate motor-cargo binding via enhancing SYD-2's association to UNC-104. SYD-2 is known to coordinate motor organization on the synaptic vesicle membrane in turn regulating anterograde cargo transport [63].

More importantly, we further validated the effect of UNC-10 and RAB-3 on UNC-104 and SYD-2 interactions using bimolecular fluorescence complementation (BiFC) assay, a method used to study protein-protein interactions in live worms. Here, UNC-104 and SYD-2 are fused to a non-fluorescent YFP (Venus) hybrid also known as "split YFP", containing two protein (split) fragments VN and VC. If the two proteins are located close to each other (less than 7 nm apart) fluorophore complementation occurs emitting yellow fluorescent signals. Noticeably, the distribution patterns of BiFC signals (Figure 2C+D) revealing the interactions of UNC-104 and SYD-2 are quite comparable to colocalization studies that also exhibit robust effect on UNC-104

and SYD-2's colocalization in the absence of UNC-10 and RAB-3 (compare Figure 2A+B with Figure 2C+D). In wild-type worms, SYD-2 and UNC-104 displays high fluorescence intensity, however, in *unc-10* and *rab-3* mutants' fluorescence complementation between SYD-2 and UNC-104 is significantly affected (Figure 2C+D).

These data strongly supports our hypothesis that the functional interaction between UNC-104 and SYD-2 is impeded in the absence of other active zone proteins UNC-10 and RAB-3 thereby affecting the motor's trafficking property.

Effect of SYD-2/UNC-10/RAB-3 on UNC-104 cluster

Based on the results above that revealed a role of UNC-10 and RAB-3 on UNC-104's binding to SYD-2, we now sought to investigate the effect of SYD-2/UNC-10/RAB-3 on UNC-104's cluster pattern. Previously, our group reported that UNC-104 clusters along axons in an arrangement that does not match known *en passant* synapse patterns, and also demonstrated that those clusters were dynamic structures rather than inactive motor aggregates [64]. Also, it is well known that UNC-104 interacts with SYD-2 via the SAM domain, SYD-2 interacts with UNC-10 via the C_2B domain and RAB-3 interacts with UNC-10 via the N-terminal zinc finger motif thereby forming an interaction chain. Owing to the scaffolding functions of both SYD-2 and UNC-10, we wondered how the whole tripartite complex (SYD-2/UNC-10/RAB-3) would affect UNC-104 cluster patterning (Figure 3). Inspecting the axonal cluster pattern of UNC-104 in sublateral neurons of *syd-2*, *unc-10* and *rab-3* mutants, respectively, we found that loss of both, *syd-2* and *unc-10* leads to severely reduced UNC-104 cluster (Figure 3A+B). However, loss of *rab-3* does not indicate any significant effect. Moreover, not only the cluster area but also the number of

clusters per 100 µm is reduced in both *syd-2* and *unc-10* mutants while the number of clusters increases in *rab-3* mutants respectively (Suppl. Table S1).

Next, we investigated UNC-104 axonal cluster in ALM neurons of *syd-2*, *unc-10* and *rab-3* mutant animals (Figure 3C). We observed, that loss of *syd-2*, *unc-10* and *rab-3*, respectively, indeed affects the cluster area (size) (Figure 3E and Suppl. Table S2). In addition, the distance travelled by UNC-104 particles from axonal hillock to distal segments of ALM neuron is also reduced in both *syd-2* and *unc-10* mutants, however *rab-3* mutants did not show any significant effect when compared to wildtype (Figure 3D and Suppl. Table S2). From, these data it is evident that UNC-104 particles appear more proximal as opposed to the distal region in *syd-2* and *unc-10* mutant backgrounds. As an increase in stationary motors along axons likely indicates reduced motor moving properties, we thoroughly investigated the motility properties of UNC-104 in *syd-2*, *unc-10* and *rab-3* mutants.

UNC-10 and RAB-3 positively affects the motility characteristics of UNC-104

As there seem to be a direct link between UNC-104/SYD-2 with UNC-10 and RAB-3, we next asked if UNC-10 and RAB-3 containing vesicles would affect UNC-104's motility. To track UNC-104 we tagged its C-terminal with mRFP that is reported to be monomeric with less aggregation properties as opposed to GFP [65]. We carried out most of our study in ALM neurons (mechanosensory neurons) with long and well-defined axons to better characterize long-range transport. As a result, we determined that in both *unc-10* and *rab-3* mutants UNC-104's transport speed was significantly affected (Figure 4A and Suppl. Table S3) supporting our hypothesis that there is certainly a direct link between SYD-2/UNC-10/RAB-3 with UNC-104. Moreover, *syd-2 (ok217)* single mutants and *syd-2(ok217);unc-10* knockdown (a double mutant in terms that we

knocked down *unc-10* in a *syd-2* knockout worm) also does not indicate any significant difference from one another, suggesting that these two scaffolding proteins may act in the same pathway [37]. In contrast, *rab-3(js49)* single mutants and *rab-3(js49);syd-2* knockdown worms exhibited significant difference from each other. The effect is more pronounced in the absence of both SYD-2 and RAB-3 pointing to a synergistic role of these motor regulators. More interestingly, *unc-10 (md1117);rab-3(js49)* double mutants display more severe reduction in UNC-104's speed than *rab-3* single mutants. However, contrastingly, the effect of double mutant is similar to that of *unc-10* single mutants pointing to the notion that this strong effect of UNC-10 on UNC-104's motility may be due to its scaffolding function. Additionally, we could also successfully rescue the effect of *syd-2, unc-10 and rab-3* on UNC-104 motility by overexpressing these proteins in their respective mutant backgrounds.

Besides motor's speed, other parameters such as run length, persistency of movement and pausing are also largely affected in *syd-2*, *unc-10* and *rab-3* mutants. Although, single mutants did not show any robust effect on UNC-104's anterograde run length, *rab-3(js49);syd-2* knockdown as well as *unc-10;rab-3* double mutants displayed a dramatic decrease in UNC-104's run length as opposed to its single mutant counterparts (Figure 4B and Suppl. Table S3). On the other hand, overexpression of *syd-2* elevates the motor's anterograde run length, while knockdown of *unc-10* does not affect this phenomena. Moreover, we also studied the relationship between motor's anterograde moving persistency and pausing. From our results, it is evident that the persistency of motor movements dramatically increases in all mutant backgrounds (Figure 4C and Suppl. Table S4), while its pausing decreases (Figure 4D and Suppl. Table S4), suggesting that if the velocity of the motor decreases, the motor may remain attached to the microtubule for prolonged periods of time thereby reducing its pausing efficiency and hence its run length remains unaffected. In

conclusion, these results suggest that SYD-2/UNC-10/RAB-3 are required to regulate UNC-104's trafficking.

SYD-2/UNC-10 combination is required for RAB-3 transport but not for SNB-1

If UNC-104's binding to RAB-3-containing vesicles is strengthened by our hypothetical linker, then eliminating certain parts of this linker should affect the transport efficiency of these vesicles. Indeed both, *syd-2* knockout and *unc-10* knockout markedly affected the transport of RAB-3-containing vesicles (Figure 5B). However, regarding the transport of SNB-1-containing vesicles, their transport is only affected by *syd-2* knockout worms (Figure 5A). Besides the speed, the run length of RAB-3-containing vesicles are also largely affected in *syd-2* and *unc-10* mutants (Figure 5D). Similar to the tendencies observed for SNB-1 velocity, run length is also affected only in *syd-2* mutant background (Figure 5C). These results strongly implicate that a SYD-2/UNC-10 combination is important for RAB-3 transport but not for SNB-1 transport.

We then sought to understand if RAB-3 and SNB-1 are in the same transport system as other comparable cargoes such as syntaxin. Interestingly, knockdown of *rab-3* on *snb-1::mrfp* expressing worms did not exhibit any SNB-1 transport defect (Figure 5A). Similarly, the knockdown of *snb-1* on *mcherry::rab-3* expressing worm (Figure 5B) also did not show any significant defect suggesting that synaptobrevin (SNB-1) is transported independently from RAB-3. (Also see Suppl. Table S5 for raw data of Figure 5A-D).

Cargo accumulation in ALM neurons

Similar to the motility pattern as observed for SNB-1 and RAB-3 containing vesicles, we then examined SNB-1 and RAB-3 cargo accumulation in *syd-2* and *unc-10* mutants, respectively. For SNB-1 containing vesicles, it is evident that these vesicles travelled for shorter distances (from

axonal hillock to distal areas: Figure 5E) in *syd-2* mutants (Figure 5E+F). In contrast, the average distance travelled by RAB-3 vesicles was significantly affected in both *syd-2* as well as *unc-10* mutants indicating that the synaptic vesicle marker RAB-3 accumulates in the proximal regions of ALM neurons rather than being transported to the distal segments (Figure 5G+H). Another attractive finding is that the overall distance travelled by SNB-1 is much shorter compared to RAB-3 (compare Figure 5F and 5H). These data also lead to the above mentioned conclusion that SYD-2/UNC-10 combination is required for RAB-3 transport to the synapse, while only SYD-2 is sufficient to transport SNB-1 containing vesicles. (Also see Suppl. Table S6 for raw data of Figure 5F+H).

Role of PH domain in regulating the interaction of UNC-104 with SNB-1 and RAB-3

In another approach, we wish to understand to which extent colocalization between UNC-104 and SNB-1, as compared to UNC-104 and RAB-3, would change when eliminating UNC-104's PH domain. If an additional linker between RAB-3 and UNC-104 exists, then the deletion of UNC-104's PH domain (known to link the motor to the vesicle membrane) would affect the colocalization to a much lesser extent compared to SNB-1 and UNC-104. Interestingly, data from Figure 6E clearly shows changes in colocalization between SNB-1 and UNC-104 before and after deleting the PH domain. Motor and cargo visibly indicate reduction in the degree of colocalization in the absence of PH domain (Figure 6E+F) suggesting that the PH domain is the only binding site for the motor to the SNB-1 containing vesicle.

Also, as hypothesized, the interaction between UNC-104 and RAB-3 was affected to a much lesser extent in the absence of UNC-104's PH domain (Figure 6A-D). Further, it would be of interest to investigate the UNC-104/RAB-3 interaction by deleting parts of the linker. As expected,

in *syd-2* and *unc-10* mutants the colocalization between UNC-104 and RAB-3 is reduced confirming our proposed idea that an additional linker of SYD-2/UNC-10 is present that additionally strengthens the interaction of UNC-104 to its cargo RAB-3 (Figure 6C+D). Another attractive finding is that the interaction between SNB-1/UNC-104 did not display any significant reduction in the absence of UNC-10 (Figure 6E+F). Thus, UNC-10 might serve as a scaffold for RAB-3 containing vesicles but not for SNB-1. Additionally, we also observed the colocalization of UNC-104/SNB-1 and UNC-104/RAB-3 in the absence of PH domain in dorsal and ventral cord neurons (Figure 6G+H). Interestingly, the result is consistent with the data shown in Figure 6A-F. (Also see Suppl. Figures S2 and S3 for colocalization related line scans).

Previous studies claim that synaptic vesicles precursors might be transported and packed in independent vesicles [59], therefore we also examined the interaction of SNB-1 and RAB-3 via bimolecular fluorescence complementation assay (Figure S1C). It is notable that RAB-3/SNB-1 complex was found to only emit visible fluorescence in the cell body of amphid neurons and this complex also colocalizes with UNC-104 in somas. One possibility is that BiFC is indeed sensitive enough that even weak and transient protein interactions can be detected. Also it could be possible that these synaptic vesicle proteins (SNB-1 and RAB-3) are sorted into different vesicles in cell bodies [59] therefore we could see their colocalization in the cell bodies in Figure S1C.

Discussion

The multiple binding sites of active-zone proteins have been extensively studied. For instance, liprin-α contains (besides LAR and KIF1A/UNC-104) also binding sites for RIM/UNC-10, CAST and GIT. RIM/UNC-10 itself encompasses a RAB-3, liprin-α, Munc-13 and CAST binding sites [66]. Based on this knowledge, we proposed a model in which Rab-3 containing vesicles (but not SNB-1 containing vesicles) would benefit from an additional linkage that supports its connection to the motor UNC-104 (Figure 7). As mentioned above, transport selectivity via specific motor receptors are well discussed in the literature. Therefore, we assume that this tripartite linkage of SYD-2/UNC-10/RAB-3 complex may act as a novel receptor for UNC-104 to selectively transport RAB-3 containing vesicles. However, SNB-1 is transported by both UNC-104 and UNC-116 and specific receptors for its transport still needs to be identified.

We indeed may assume that the classical linkage of UNC-104 to vesicular structures via its PH domain [23] is weak and non-specific [62] and that our proposed linker would provide the motor additional connectivity and strength. Importantly, reports exist that liprin-α/SYD-2 affects the transport of dense-core vesicles [44] and RIM1α/UNC-10 (known to be a dense-core vesicle protein) as well as RAB-3 are mislocalized in *liprin-α/syd-2* mutants. It is also known that UNC-104 transports dense-core vesicles [15] which is interesting to further comprehend whether this linker is specific to synaptic vesicles only or if it also applies to dense core vesicles. Additionally, literature evidences also suggests that SYD-2/UNC-10, UNC-10/RAB-3 and SYD-2/RAB-3 colocalize and co-transport with each other [45] consistent with the fact that all these three active zone proteins may either directly or indirectly impede UNC-104's trafficking behavior. Therefore, an evidence of a physical interaction between SYD-2, UNC-10 and RAB-3 affecting UNC-104's transport would further help to understand this mechanism.

Effect of UNC-10 and RAB-3 on SYD-2's binding to UNC-104.

To prove that our proposed model is correct, we first investigated whether UNC-10 and RAB-3 would play a critical role in the UNC-104/SYD-2 complex. SYD-2 is known to positively regulate the clustering and transport of monomeric UNC-104, thereby enhancing its activity [29]. Thus, we asked whether UNC-10 and RAB-3 would affect SYD-2's binding to UNC-104. Indeed, precipitating UNC-104::GFP from whole worm lysates, SYD-2 levels were reduced in *unc-10 (e102* point mutation as well as *md1117* knockout*)* mutant alleles (Figure 1E+F). It can be speculated that loss of UNC-10 may cause UNC-104 to return to its monomeric configuration thereby affecting the binding of SYD-2. It is also possible that UNC-10 acts as a stabilizer of SYD-2 by facilitating its oligomerization, as UNC-10 binds to C-terminal of SYD-2 [36 67]. The importance of oligomerized SYD-2 lies in its proposed function as a scaffolding protein that can bind to more than one UNC-104 (via its SAM) at the same time [38, 45].

Similarly, precipitating UNC-104::mRFP from whole worm lysates, SYD-2 levels were also reduced in *rab-3(js49)* mutant animals (Figure 1G+H). UNC-104 requires *arl-8* a small GTPase to unlock its auto inhibitory state [68]. ARL-8 is usually bound to the cargo vesicle, therefore it is possible that in the absence of RAB-3 the motor cargo association is compromised causing inactivation of UNC-104. Thereby, the binding of SYD-2 is robustly affected. On the other hand, the SYD-2 expression level study (Figure 1A+B) is also consistent with our Western blot analysis (Figure 1C+D) (comparing SYD-2 intensity in western blots to SYD-2 mRNA levels). On careful observation, it can be seen that SYD-2 mRNA levels were increased in *unc-10* mutants while its expression is reduced by 50% in *rab-3* mutant, respectively (Figure 1A-D).

Our *in vivo* assays further strengthened our biochemical findings. We demonstrated that in the absence of UNC-10 and RAB-3 the colocalization between SYD-2 and UNC-104 is largely reduced in the nerve ring (Figure 2A+B). More importantly, for protein pairs, we also performed BiFC assays in which we fused hybrids of Venus to UNC-104 and SYD-2 and observed successful complementation in wild-type animals. However, in *unc-10* and *rab-3* mutants, this complementation was clearly diminished (Figure 2C+D). SYD-2 is known to promote anterograde trafficking of synaptic vesicles in axons of Drosophila and *C. elegans* [29 69]. In *syd-2* mutants, it has been shown that UNC-10 and RAB-3 mislocalize to dendrites in DA neurons [44]. Also, the loss of *syd-2*, *unc-10* and *rab-3* cause depletion of synaptic vesicles at the dense projection [37]. Owing to these interactions between SYD-2, UNC-10 and RAB-3, one may speculate, that the absence of these core proteins might have adverse effects on each other's interaction.

Antagonistic effects of UNC-10 and RAB-3 on UNC-104's clustering.

Previously, it has been reported that the lack of SYD-2 abolishes UNC-104 clusters in axons and at the same time, motors were also steered to the terminal endings [29]. Similar to this finding, we demonstrated here that the loss of UNC-10 leads to loss of UNC-104 clusters in sublateral neurons (Figure 3A+B). Consistent with this finding, we also observed that the UNC-104 cluster size is reduced in ALM neurons as well as the motor's distance travelled from the axonal hillock to distal locations is also largely diminished (Figure 3C-E). However, the loss of RAB-3 displays a rather antagonistic effect when compared to SYD-2 and UNC-10 mutations. Neither UNC-104 cluster in sublateral neurons are affected nor the anterograde distance travelled by this motor in ALM neurons (Please see Figure 3B and 3D). Strikingly, the cluster area is significantly reduced in ALM neurons (Figure 3E), in the absence of RAB-3. It could be assumed that RAB-3 does not inherit scaffolding functions as opposed to SYD-2 and UNC-10. In addition, the RAB-3 effect

could also be due to the presence of other Rabs that may exhibit partial overlapping functions with RAB-3. This notion could be supported by the finding that RAB-27 is a close homolog of RAB-3 and is also regulated by AEX-3/DENN/MADD in *C. elegans* [56 59]. Another possibility could be that some synaptic vesicle proteins are transported in a RAB-independent fashion [59]. We further deduce that motor cluster may act as "stations" along the lengthy *C. elegans* axons (up to 0.5mm) to exchange inactive motors for active motors on paused cargos. This assumption is in accordance with a recent study demonstrating that AZ assembly proteins maintains the stability of synaptic-vesicle cluster and further regulate the synaptic vesicle transport in *C. elegans* [46]. Interestingly, synaptic vesicle proteins also maintain synaptic vesicle clusters when the anterograde transport is compromised. It is also noteworthy that a JNK pathway acts in parallel to UNC-104 that functions as an effector of ARL-8 and controls the clustering of synaptic vesicles and active zone proteins at the presynaptic terminals [45].

The role of the tripartite linker in facilitating UNC-104's transport characteristics.

SYD-2 positively regulates UNC-104's moving characteristics [29]. As our hypothesis suggests that UNC-104 might use an additional linker (SYD-2/UNC-10/RAB-3) to connect to the vesicle, it is imperative to understand the role of these active zone proteins on its transport behavior. At first, we found that UNC-10 not only altered the cluster pattern of UNC-104 but from Figure 4A it is evident that UNC-104's anterograde velocity is severely reduced in *unc-10* mutant background. Also, the moving persistency (Figure 4C) (indicating the overall moving direction and motor's active state) as well as pausing (Figure 4D) are clearly affected. Though it is hard to comprehend how this indirect interaction between UNC-104 and UNC-10 would induce such obvious effects on UNC-104's motility, we assume that UNC-10 might regulate SYD-2's binding to UNC-104. This finding is supported by the observation that changes in motility as well as cluster pattern of

UNC-10 are similar to those observed in *syd-2* mutants. Moreover, we demonstrated that UNC-10 RNAi knockdown on *syd-2* mutants did not show any severe effect as opposed to *syd-2* single mutants. This data suggests that these two proteins act in the same pathway to regulate synaptic vesicles and this result is also consistent to a previous report [37]. On the other hand, overexpression of SYD-2 elevated the run length in anterograde directions, however, UNC-10 knockdown did not affect this phenomenon. Therefore, we speculate that localization of UNC-10 to the active zone via UNC-104 transport may be controlled by the scaffolding protein SYD-2.

From another study, it is obvious that KIF1A is indispensable for the transport of both, DENN/MADD and RAB3, whereas DENN/MADD preferentially binds to GTP-activated RAB3 that regulates axonal transport [59]. As the relationship of UNC-104 and RAB-3 is well described in our study, we sought to understand the effect of *rab-3* mutants on UNC-104's motility. We determined, that in *rab-3* mutant animals, the anterograde speeds and pausing was largely reduced, while moving persistency elevated (Figure 4), consistent with the finding that KIF1A biochemically associates with RAB-3 carrying vesicles (Figure 1). Additionally, overexpressing RAB-3 in *rab-3* mutant worms rescued UNC-104's motility pattern to wild-type levels. In contrast, *rab-3(js49)* single mutants and *rab-3(js49);syd-2* knockdown worms exhibit significant differences from each other (Figure 4). The effect is indeed more pronounced in the absence of both SYD-2 and RAB-3 (Figure 4) pointing to a synergistic role of these motor regulators. Moreover, the effect of *unc-10; rab-3* double mutants on UNC-104's anterograde speeds are similar to *unc-10(md1117)* single mutants but more severe as compared to *rab-3* mutant worms. Besides negatively affecting UNC-104's velocity parameters, these double mutants also display a strong effect on the motor's run length indicating a severe reduction, as opposed to both *unc-10* and *rab-3* single mutants (Figure 4B). These results are comparable to a former study that dissected

the direct interactions between RAB-3 and RIM suggesting epistatic regulation by UNC-10 and RAB-3 [70].

Note that the speed fluctuations are generally smaller when compared to the run length. It is important to know that the motor's run length is indeed affected by a variety of parameters especially the microtubule binding proteins and the length of microtubules, respectively [71]. Therefore, from our study it is evident that SYD-2/UNC-10/RAB-3 positively regulate UNC-104's transport characteristics. Collectively, the tripartite linker might act as an important stabilizer to additionally support the motor-cargo association and these data also reveal the binding dependencies of UNC-104 on the proposed SYD-2/UNC-10/RAB-3 linker.

SYD-2/UNC-10 combination is selectively required to transport RAB-3 containing vesicles.

We have demonstrated above that the SYD-2/UNC-10/RAB-3 linker positively regulates UNC-104's transport behavior. It would be intriguing to understand how SYD-2/UNC-10 complex modulates the binding of UNC-104 to RAB-3 containing vesicles. If UNC-104's binding to RAB-3 is indeed strengthened by the SYD-2/UNC-10 complex, then eliminating the parts of the linker should affect the transport efficiency of vesicles. Indeed, *syd-2* knockout and *unc-10* knockout largely affected the transport of RAB-3 containing vesicles, however regarding the transport of SNB-1 containing vesicles, their transport was only affected by *syd-2* mutants (Figure 5A+B). This result strongly supports our hypothesis that SYD-2/UNC-10 combination is selectively required for RAB-3 transport but not SNB-1 transport. Also, SNB-1-tagged vesicle speeds in the absence of *rab-3* remain unaffected, similarly, this is also applicable to RAB-3-tagged vesicles whose moving speeds are not affected by *snb-1* knockdown (Figure 5A+B). This is consistent with the notion that other synaptic vesicle precursors are transported independently of RAB-3, as they are

sorted into different vesicles in somas and are co-assembled at the synaptic terminals (Suppl. Figure S1C) [59]. Another interesting finding is the overall movement of SNB-1 which is slower and remains at shorter distances when compared to RAB-3 (Figure 5E-H). Consequently, this observation also fits to our model in which multiple motors can be restricted to the vesicular surface by tight interactions with cargo molecules that can therefore move for longer distances as opposed to a single proccessive motor [72]. It is also worth mentioning that UNC-104 undergoes dimerization and is activated only upon cargo binding [73 74], and that's why may be an additional linker could support UNC-104 and keep it in an activated state. Taken together, these results suggest an important regulatory role of UNC-104 in cargo distribution. When the anterograde synaptic vesicle trafficking machinery is disrupted, synaptic vesicle markers accumulate in the soma and proximal regions of neurons [75]. Particularly, in *syd-2* and *unc-10* mutants the run length of RAB-3, as well as the average distances travelled by RAB-3, appears to be more at the proximal region affecting its synaptic localization.

The role of PH domain in motor-cargo interaction and how this interaction could be strengthened by an additional linker.

Pleckstrin homology domains are composed of 120 amino acids and are found in more than 100 different proteins studied so far. They have been found to be involved in various intracellular signaling processes, cytoskeletal organization, intracellular membrane transport and membrane phospholipid modification [76-80]. Most of the proteins bearing PH domains interact with cellular membranes by binding to phosphoinositide's respectively [81]. Specific recognition of phosphoinositide is a characteristic property of only a few PH domains. There might be a general attraction to the membrane surface in order to support other specific regulatory interactions [82]. The roles of membrane lipids in motor-driven transport has received less attention, therefore *in*

vitro-motility assays were used by others to investigate the role of UNC-104 in the transport of membrane cargo. Earlier reports suggest, that lipid raft formation plays an essential role in regulating the vesicle transport by monomeric UNC-104 being able to bind to the phosphatidylinositol (4, 5) bisphosphate (PtdIns(4,5)P_2) containing liposomes via its PH domain [73]. Two regulatory mechanisms could activate the membrane transport. (1) Several monomeric UNC-104 motors could cluster on the membrane surface thereby promoting microtubule attachment and initiate transport. (2) UNC-104 could dimerize in solution via its coiled coil regions, thus transport would be enhanced by hand-over-hand mechanisms (as opposed to biased diffusion of the monomeric motor). Mostly, the binding of the PH domain to phosphoinositide's are weak and non-specific, and this selectivity can also be modulated by sequence changes [62]. In addition, the strength of the lipid-protein interaction also depends upon the lipid constituents that decrease in the order of phosphatidic acid> phosphatidylserine>phosphatidylinositol [83]. Further, they suggest that the affinity of protein-lipid binding between protein lipase C delta 1 and PI (4,5) P_2 can be influenced by membrane charge with phosphatidylserine causing a conformational change in the PH domain thereby affecting the membrane binding affinity of protein lipase C [83]. Therefore, although this protein-lipid interaction seems imperative with varying specificity, other vesicle-associated proteins could also mediate UNC-104-related transport. It is of profound importance to identify these vesicle-associated proteins. In our study, we hypothesized that an additional linker of RAB-3/UNC-10/SYD-2 is likely present and is necessary to enhance the motor-cargo connectivity. In the presence of this linker, UNC-104 selectively binds to RAB-3-containing vesicles.

As the PH domain connects the motor to its cargo, it would be fascinating to know if its absence affects UNC-104's interaction to its cargo. From our result, it is evident that upon PH domain

deletion UNC-104's binding to RAB-3 remains unaffected, although contrasting regulation was seen between UNC-104 and SNB-1 (compare Figure 6A+B+D to 6E+F) as expected (SNB-1 does not interact with UNC-10, Figure 6E+F). If the additional linker is enhancing the motor cargo connectivity, removing parts of the linker should diminish the UNC-104/RAB-3 interaction. As expected, in the absence of SYD-2 and UNC-10, UNC-104 (with a deleted PH domain) and RAB-3 binding was markedly reduced (Figure 6C+D).

Methods and Materials

RNA isolation

Worms were washed thrice with M9 buffer and then Trizol was added to disrupt the membrane. The samples were stored at -80°C overnight. The following day, samples were thawed and centrifuged at 14,000 rpm for 10 mins at 4°C. The supernatant was transferred to an RNase-free Eppendorf tube. Under the hood, 50 µl of chloroform was added and the samples were vortexed for 30 secs followed by 3 min incubation at room temperature. The standing samples were then centrifuged at 12,000 rpm for 15 mins at 4°C. A clear top layer was transferred to an Eppendorf tube without disturbing the other layers. The process is repeated again until a clear RNA layer was obtained. This solution was then treated with 125 µl isopropanol and inverted several times. The samples were then spun down at 12,000 rpm for 10 mins at 4°C. The supernatant is discarded and the pellet is then treated with 70% ethanol (diluted in DEPC water). After centrifugation at 12,000 rpm for 5 mins at 4°C, the RNA pellet was air-dried and dissolved in 10 µl of DEPC water and stored at -80°C for future use.

cDNA synthesis

"Superscript® III first-strand synthesis system for RT-PCR" cDNA synthesis kit (Invitrogen, NY,USA) was used to isolate cDNA from worms. Samples were prepared by mixing 8 µl of mRNA with 1 µl of either oligo (dT) or random hexamer primer along with 1 µl of annealing buffer. Incubate the samples at 65°C for 5 mins and immediately place it on ice for 1 min. Next, add the cDNA synthesis enzyme mix into the RNA sample mixture. Finally incubate them at 50°C for 50 mins and terminate the reaction with 5 mins of incubation at 85°C respectively. The synthesized cDNA was then used to clone the *rab-3* constructs and RT-PCR was performed to identify the expression levels of *syd-2*.

Real-time PCR

To evaluate *syd-2* RNA levels in *unc-10* and *rab-3* mutants (Figure 1A+B), we performed real-time PCR assays employing ABI StepOne Plus Real time PCR system in conjunction with the ABI Power SYBR green PCR master mix. RNA levels of *syd-2* were normalized to *cdc-42* internal control. The following primers were used: CGGAACAATACTCGACTTC (forward) and GCCACACGCTCCATT (reverse) that includes a part of 2nd and 4th exon (200 bp) for *syd-2* and CTGCTGGACAGGAAGATTACG (forward) and TCGGACATTCTCGAATGAAG (reverse) for *cdc-42.*

RNAi feeding assay

NGM plates containing ampicillin (25 µg/ml) and 1 mM IPTG were inoculated with HT115 *E. coli* strain carrying the appropriate dsRNA clone (UNC-10: X-3F06, SYD-2: X-5K09), and grown overnight. Fifteen to twenty worms were transferred to RNAi feeding plates and incubated at 20˚C. Worms were then transferred to new RNAi feeding plates every 24 hours and the F1 progeny was

used for analysis after day 5. As control, worms were fed with HT115 bacteria containing L4440 empty vector.

Protein harvesting, extraction and quantification

To extract proteins from worms, we prepared lysates from young adults (72 h) based on a previously described protocol [84]. Worms were washed thrice with 0.1N NaCl solution followed by sucrose floatation. The floating worms were then collected and washed 2X times with cold water followed by a wash with HB buffer without DTT and protease. Finally, 3X volume of HB with DTT and protease inhibitor was added and the sample was stored at -80˚C. The harvested worms are then subjected to French press to extract the protein. The protein quantification is done using commercial BCA Kit.

Western blotting and Co-Immunoprecipitation Assays

To perform Western blotting from whole worm lysates, we employed the protein extracted from section 2.5 above. 100 µg sample protein was used and membrane blocking was carried out using milk powder for 1-1.5 hours at room temperature (RT). Primary goat N-terminal anti-SYD-2 antibody (cL-19 #sc-15655, Santa Cruz) was incubated at 4°C for 14 hours at 1/500 dilution. The secondary anti-goat antibody was incubated at RT for 2 hours with 1/1000 dilutions. Anti β-Actin antibody was used as control (sc-47778, Santa Cruz). Similarly, One mg protein extract was used for immunoprecipitation and incubated with protein G beads and 4 µg mouse anti-GFP antibody (B-2 #sc-9996, Santa Cruz). After treatment worm lysates were detected by western blotting with a 1:500 dilution of the anti-SYD-2 antibody (primary antibodies dilutions based on the manufacturer's suggestion). Band density analysis was done using NIH ImageJ 1.50 software based on a method published by Schneider et al. [85]. (Please see Figure 1E-H)

Mutant worms used in this study

N_2 is the wild-type *C.elegans* strain received from Caenorhabditis Genetics Center (CGC, Minnesota, USA). ZM607 *(ok217)* carries a large deletion covering most of the N-terminal coiled coils in *syd-2* gene. It leads to an ochre stop codon after 200 amino acids [29]. NM1657 *(md1117)* carries an 8601 bp deletion in *unc-10* gene that includes the entire coding region along with a part of 5' and 3' UTR's. This mutant exhibits mild uncoordinated movements that resemble a coiler [48]. CB102 *(e102)* is a C to T substitution in intron 15 of *unc-10* gene that leads to a splicing defect and produces a truncated protein that excludes the C-terminal domain [48]. NM791 *(js49)* is a G to A transition in position 2 of tryptophan 76 codon in *rab-3* gene that encodes a nonsense mutation leading to a premature stop [30].

***C.elegans* strains and plasmids**

Worms were maintained at 20°C on NGM agar plates seeded with OP50 *E. coli* according to standard methods [86]. Transgenic animals *Punc-104::unc-104::gfp(e1265), Punc-104::unc-104ΔPH::gfp(e1265), Punc-104::unc-104::mrfp(e1265) and Punc-104::unc-104::mrfp(ok217)* were described previously [21 29]. The existing constructs *Punc-104::unc-104::gfp* and *Punc-104::unc-104::mRFP* were microinjected at a concentration of 100 ng/µl into *unc-10(md1117)* and *rab-3(js49)* mutants worms to generate transgenic lines *unc-10(md1117);nthEx[Punc-104*::*unc-104::mrfp], unc-10 (md1117);nthEx[Punc-104*::*unc-104::gfp] and rab-3(js49);nthEx[Punc-104*::*unc-104::mrfp]* respectively. All the mutant strains were received from the Caenorhabditis Genetics Center (Minnesota, USA).

For colocalization studies, the existing plasmid *Punc-104::gfp::syd-2* was coinjected along with *Punc-104::unc-104::mrfp* (each at a concentration of 75 ng/µl) into N2 wild type animals, *unc-10(md1117)* and *rab-3(js49)* mutants animals to obtain strains N2;*nthEx[Punc-104::gfp::syd-*

2;Punc-104::unc-104::mrfp], *unc-10 (md1117)*;*nthEx[Punc-104::gfp::syd-2;Punc-104::unc-104::mrfp]* and *rab-3(js49)*; *nthEx[Punc-104::gfp::syd-2;Punc-104::unc-104::mrfp]*. Likewise, *Punc-104::gfp::syd-2* (75 ng/µl) was microinjected into *unc-10(md1117);rab-3(js49)[Punc-104::unc-104::mrfp]* to obtain *unc-10(md1117),rab-3(js49)*; *nthEx[Punc-104::gfp::syd-2;Punc-104::unc-104::mrfp]*. For BiFC (biomolecular fluorescence complementation) studies, the following strains were generated using the existing plasmids *Punc-104::unc-104::VC155* and *Punc-104::VN173::syd-2* [64]: N2;*nthEx[Punc-104::unc-104::VC155;Punc-104::VN173::syd-2]*, *unc-10(md1117)*;*nthEx[Punc-104::unc-104::VC155;Punc-104::VN173::syd-2]* and *rab-3(js49); nthEx[Punc-104::unc-104::VC155;Punc-104::VN173::syd-2]* respectively.

Further *rab-3* rescue strains were generated by cloning *Punc-104::yfp* transcriptional reporter followed by insertion of *rab-3* gene to create *Punc-104::rab-3::yfp* translational fusion. To clone *Punc-104::yfp*, we amplified YFP sequence using the forward primer AAAAAAGGTACCGGTAGAAAAAATGAGTAAAGGAGAAGAACTTTT and reverse primer AAAAAAGAATTCTACGAATGCTATTTGTATAGTTCATCCATGCCA and then substituted *gfp* in *pPD95.77::Punc-104:: gfp* vector with *yfp*. Next, we sub cloned *rab-3* gene into *Punc-104::yfp* transcriptional fusion by amplifying *rab-3* cDNA using CTCTAGAGGATCCCCATGAATAATCAACAGGCTGCCA forward primer and CCTTTGGCCAATCCCTTGCAATTGCATTGC reverse primer using the FuseIn™ cloning technique. The plasmid was then injected at 75 ng/µl into *rab-3(js49);nthEx[Punc-104*::*unc-104::mrfp]* mutant strain to create rescue transgenic lines *rab-3(js49);nthEx[Punc-104*::*unc-104::mrfp; Punc-104::rab-3::yfp]*.

Likewise, *unc-10* rescue strains were generated by cloning unc-10 gene in *pPD95.77::Punc-104:: gfp* vector using CTCTAGAGGATCCCCATGGACGATCCGTCGATGATGCC (forward) and

CCTTTGGCCAATCCCctgctgaGCACCTCC (reverse) primers employing the FuseIn™ cloning technique. The plasmid was then injected at 75 ng/µl into *unc-10(md1117);nthEx[Punc-104*::*unc-104::mrfp]* mutant strain to create rescue transgenic lines *unc-10(md1117);nthEx[Punc-104*::*unc-104::mrfp; Punc-104::unc-10::gfp]*.

Next, the *syd-2* rescue strains were obtained by coinjecting the existing plasmid *Punc-104::gfp::syd-2* along with *Punc-104::unc-104::mrfp* (each at a concentration of 75 ng/µl) into *syd-2(ok217)* mutant worms to get *syd-2(ok217)*;*nthEx[Punc-104::gfp::syd-2;Punc-104::unc-104::mrfp*] respectively.

rab-3 was amplified from cDNA libraries with primers ATGGCGGCTGGCG-GACAA (forward) and TTAGCAATTGCATTGCTGTT (reverse). We then added restriction sites with primers AAAAGCTAGCATGGCGGCTGG-CG (forward) and AAAACCATGGTTAGCAATTGCATTGCTGTT (reverse). PCR was performed using *Taq* DNA polymerase (New England Biolabs). PCR products were ligated into the yT&A cloning vector (Yeastern Biotech). After NheI and SalI digestion, *rab-3* was ligated to the destination vector *Punc-104::mcherry::GW* to obtain *Punc-104::mcherry::rab-3*.

In order to generate, cargo transgenic lines we injected existing constructs *Punc-86::snb-1::mRFP* [29] and *Punc-104::mcherry::rab-3* into N2 wild type animals, *unc-10(md1117)* and *syd-2(ok217)* mutants (at a concentration of 100 ng/µl) to obtain strains N2;*nthEx[Punc-86::snb-1::mRFP],* N2;*nthEx[Punc-104::mcherry::rab-3], syd-2(ok217);nthEx[Punc-86::snb-1::mRFP], syd-2(ok217); nthEx[Punc-104::mcherry::rab-3], unc-10(md1117);nthEx[Punc-86::snb-1::mRFP] and unc-10(md1117); nthEx[Punc-104::mcherry::rab-3].*

Likewise, for UNC-104 and RAB-3 colocalization studies, the existing plasmids *Punc-104::unc-104ΔPH::gfp* and *Punc-104::mcherry::rab-3 were coinjected into* N2 wild type animals, *unc-10(md1117)* and *syd-2(ok217)* mutants to generate N2;*nthEx[Punc-104::unc-104ΔPH::gfp; Punc-104::mcherry::rab-3], unc-10(md1117)*;*nthEx[Punc-104::unc-104ΔPH::gfp;Punc-104::mcherry::rab-3]* and *syd-2(ok217);nthEx[Punc-104::unc-104ΔPH::gfp;Punc-104::mcherry::rab-3]* respectively.

Punc-104::rab-3::VN173 and *Punc-104::snb-1::VC155* plasmids were generated by amplifying *rab-3* cDNA using GGCGCGCCATGAATAATCAACAGGC forward primer with AscI site and ACCGGTGCAATTGCATTGCTGTTGAG reverse primer with AgeI site and substituted *map-1* insert in *Punc-104::map-1::VN173* plasmid with *rab-3*. At the same time, *snb-1* genomic DNA was amplified using GGCGCGCCATGGACGCTCAAGGAGATGC forward primer with AscI site and GGTACCTTTTCCTCCAGCCCATAAAACGATGA reverse primer with KpnI site and substituted *lin-2* in *Punc-104::lin-2::VC155* plasmid with *snb-1*. These plasmids were then coinjected (80 ng/µl) into N2 worms to generate N2;*nthEx[Punc-104::rab-3::VN173; Punc-104::snb-1::VC155] to* investigate BiFC.

Unc-10(md1117) and *rab-3(js49)* double mutants were generated by crossing *unc-10 (md1117);nthEx[Punc-104*::*unc-104::mrfp]* expressing male worms with *rab-3(js49)* hermaphrodites. Red fluorescent males from F1 generation exhibiting coiler phenotype were back-crossed into *rab-3 (js49)* F_0 hermaphrodites to obtain *unc-10(md1117);rab-3(js49)* homozygous animals.

Worm imaging and motility analysis

For microscopic observations, worms were immobilized on 2% agarose-coated cover slides, and no anesthetics (e.g., levamisole) were used (reported to affect motor motility [87]). A Zeiss

LSM780 confocal laser scanning microscope was employed for imaging worms as shown in Figures 2 and 6. For motility analysis (Figure 4) and further imaging (figure 3 and 5) , we employed an Olympus IX81 microscope with a DSU Nipkow spinning disk unit connected to an Andor iXon DV897 EMCCD camera for high-resolution and high-speed time-lapse imaging at 4-5 frames per second. To convert recorded time-lapse sequences into kymographs, we used the imaging analysis software NIH ImageJ (NIH, http://rsb.info.nih.gov/ij/). The "straighten plugin" was used to straighten curved axons, and after drawing a line over the axon, the plugin "reslice stack function" was executed to generate kymographs. In kymographs, static particles appear as vertical lines, whereas the slope of a moving particle corresponds to the velocity (speed) of the particle. A pause is defined if motors move less than 0.07 µm/s, and each calculated velocity event does not contain any pauses. On average, we analyzed approximately 600 moving events per experiment from 15 to 25 individual worms. A moving event is defined as a single motility occurrence typically right after a pause or a reversal, and an event ends when the motor again pauses or reverses.

Motor cluster analysis (Figures 3B+E) was carried out using ImageJ's "area" tool and the "particle analyze" plugin. To measure travel distances (Figures 3D and 5F+H) of particles in (straightened) neurons, we used ImageJ's "line tool" to draw a line from the proximal axon hillock to identified distal particle. Intensity Correlation Quotient (ICQ) (Figures 2B, 6D+F) was measured by selecting the region of interest using the "polygonal selection tool" in ImageJ. After background fluorescent intensity subtraction (ImageJ→Process→Subtract Background), the plugin 'Intensity Correlation Analysis' was used to generate ICQ values. ICQ values range from -0.5 to 0.5, and values close to 0.5 stand for interdependent expression of two fluorophores, values close to -0.5 stand for segregated expression, and values around 0 imply random expression. For fluorescence intensity quantification (Figure 2D) the following formula was used: Integrated density of selected region

– (area of selected region * mean fluorescence of the background) [88]. Parameters such as mean grey value of background, area of selected region and integrated density of selected region was measured using ImageJ. Line scans (Suppl. Figure S2 and S3) were generated using ImageJ (ImageJ→Analyze→Plot profile) after straightening the neurite using the ImageJ plugin "straighten". Further these values from ImageJ are plotted using MS Excel.

ACKNOWLEDGEMENTS

We thank the *C. elegans* Core Facility (CECF) Taiwan (funded by the Ministry of Science and Technology, MOST) for providing microinjection setups and worm observation systems. We acknowledge MOST grant NSC 100-2311-B-007-004 to OIW and support by the Brain Research Center of National Tsing Hua University under the Higher Education Sprout Project funded by the Ministry of Science and Technology and Ministry of Education in Taiwan.

References

1. Luo L. Actin cytoskeleton regulation in neuronal morphogenesis and structural plasticity. Annu Rev Cell Dev Biol 2002;**18**:601-35 doi: 10.1146/annurev.cellbio.18.031802.150501[published Online First: Epub Date]|.
2. Barnes AP, Polleux F. Establishment of axon-dendrite polarity in developing neurons. Annu Rev Neurosci 2009;**32**:347-81 doi: 10.1146/annurev.neuro.31.060407.125536[published Online First: Epub Date]|.
3. Kapitein LC, Hoogenraad CC. Which way to go? Cytoskeletal organization and polarized transport in neurons. Mol Cell Neurosci 2011;**46**(1):9-20 doi: 10.1016/j.mcn.2010.08.015[published Online First: Epub Date]|.
4. Brouhard GJ. Dynamic instability 30 years later: complexities in microtubule growth and catastrophe. Mol Biol Cell 2015;**26**(7):1207-10 doi: 10.1091/mbc.E13-10-0594[published Online First: Epub Date]|.
5. Mitchison T, Kirschner M. Dynamic instability of microtubule growth. Nature 1984;**312**(5991):237-42
6. Niwa S. Kinesin superfamily proteins and the regulation of microtubule dynamics in morphogenesis. Anat Sci Int 2015;**90**(1):1-6 doi: 10.1007/s12565-014-0259-5[published Online First: Epub Date]|.

7. Hirokawa N, Noda Y, Tanaka Y, Niwa S. Kinesin superfamily motor proteins and intracellular transport. Nat Rev Mol Cell Biol 2009;**10**(10):682-96 doi: 10.1038/nrm2774[published Online First: Epub Date]|.
8. Perlson E, Maday S, Fu MM, Moughamian AJ, Holzbaur EL. Retrograde axonal transport: pathways to cell death? Trends Neurosci 2010;**33**(7):335-44 doi: 10.1016/j.tins.2010.03.006[published Online First: Epub Date]|.
9. Maday S, Twelvetrees AE, Moughamian AJ, Holzbaur EL. Axonal transport: cargo-specific mechanisms of motility and regulation. Neuron 2014;**84**(2):292-309 doi: 10.1016/j.neuron.2014.10.019[published Online First: Epub Date]|.
10. Brooks BR. The role of axonal transport in neurodegenerative disease spread: a meta-analysis of experimental and clinical poliomyelitis compares with amyotrophic lateral sclerosis. Can J Neurol Sci 1991;**18**(3 Suppl):435-8
11. Franker MA, Hoogenraad CC. Microtubule-based transport - basic mechanisms, traffic rules and role in neurological pathogenesis. J Cell Sci 2013;**126**(Pt 11):2319-29 doi: 10.1242/jcs.115030[published Online First: Epub Date]|.
12. Breuss M, Keays DA. Microtubules and neurodevelopmental disease: the movers and the makers. Adv Exp Med Biol 2014;**800**:75-96 doi: 10.1007/978-94-007-7687-6_5[published Online First: Epub Date]|.
13. Hall DH, Hedgecock EM. Kinesin-related gene unc-104 is required for axonal transport of synaptic vesicles in C. elegans. Cell 1991;**65**(5):837-47
14. Maeder CI, San-Miguel A, Wu EY, Lu H, Shen K. In vivo neuron-wide analysis of synaptic vesicle precursor trafficking. Traffic 2014;**15**(3):273-91 doi: 10.1111/tra.12142[published Online First: Epub Date]|.
15. Zahn TR, Angleson JK, MacMorris MA, et al. Dense core vesicle dynamics in Caenorhabditis elegans neurons and the role of kinesin UNC-104. Traffic 2004;**5**(7):544-59 doi: 10.1111/j.1600-0854.2004.00195.x[published Online First: Epub Date]|.
16. Yonekawa Y, Harada A, Okada Y, et al. Defect in synaptic vesicle precursor transport and neuronal cell death in KIF1A motor protein-deficient mice. J Cell Biol 1998;**141**(2):431-41
17. Kern JV, Zhang YV, Kramer S, Brenman JE, Rasse TM. The kinesin-3, unc-104 regulates dendrite morphogenesis and synaptic development in Drosophila. Genetics 2013;**195**(1):59-72 doi: 10.1534/genetics.113.151639[published Online First: Epub Date]|.
18. Zhang YV, Hannan SB, Stapper ZA, Kern JV, Jahn TR, Rasse TM. The Drosophila KIF1A Homolog unc-104 Is Important for Site-Specific Synapse Maturation. Front Cell Neurosci 2016;**10**:207 doi: 10.3389/fncel.2016.00207[published Online First: Epub Date]|.
19. Brady ST, Morfini GA. Regulation of motor proteins, axonal transport deficits and adult-onset neurodegenerative diseases. Neurobiol Dis 2017;**105**:273-82 doi: 10.1016/j.nbd.2017.04.010[published Online First: Epub Date]|.
20. Millecamps S, Julien JP. Axonal transport deficits and neurodegenerative diseases. Nat Rev Neurosci 2013;**14**(3):161-76 doi: 10.1038/nrn3380[published Online First: Epub Date]|.
21. Tien NW, Wu GH, Hsu CC, Chang CY, Wagner OI. Tau/PTL-1 associates with kinesin-3 KIF1A/UNC-104 and affects the motor's motility characteristics in C. elegans neurons. Neurobiol Dis 2011;**43**(2):495-506 doi: 10.1016/j.nbd.2011.04.023[published Online First: Epub Date]|.
22. Rashid DJ, Bononi J, Tripet BP, Hodges RS, Pierce DW. Monomeric and dimeric states exhibited by the kinesin-related motor protein KIF1A. J Pept Res 2005;**65**(6):538-49 doi: 10.1111/j.1399-3011.2005.00255.x[published Online First: Epub Date]|.
23. Klopfenstein DR, Vale RD. The lipid binding pleckstrin homology domain in UNC-104 kinesin is necessary for synaptic vesicle transport in Caenorhabditis elegans. Mol Biol Cell 2004;**15**(8):3729-39 doi: 10.1091/mbc.e04-04-0326[published Online First: Epub Date]|.

24. Schoch S, Gundelfinger ED. Molecular organization of the presynaptic active zone. Cell Tissue Res 2006;**326**(2):379-91 doi: 10.1007/s00441-006-0244-y[published Online First: Epub Date]|.
25. Dresbach T, Qualmann B, Kessels MM, Garner CC, Gundelfinger ED. The presynaptic cytomatrix of brain synapses. Cell Mol Life Sci 2001;**58**(1):94-116 doi: 10.1007/PL00000781[published Online First: Epub Date]|.
26. Gundelfinger ED, tom Dieck S. Molecular organization of excitatory chemical synapses in the mammalian brain. Naturwissenschaften 2000;**87**(12):513-23 doi: 10.1007/s001140050770[published Online First: Epub Date]|.
27. Rosenmund C, Rettig J, Brose N. Molecular mechanisms of active zone function. Curr Opin Neurobiol 2003;**13**(5):509-19
28. Ziv NE, Garner CC. Cellular and molecular mechanisms of presynaptic assembly. Nat Rev Neurosci 2004;**5**(5):385-99 doi: 10.1038/nrn1370[published Online First: Epub Date]|.
29. Wagner OI, Esposito A, Kohler B, et al. Synaptic scaffolding protein SYD-2 clusters and activates kinesin-3 UNC-104 in C. elegans. Proc Natl Acad Sci U S A 2009;**106**(46):19605-10 doi: 10.1073/pnas.0902949106[published Online First: Epub Date]|.
30. Nonet ML, Staunton JE, Kilgard MP, et al. Caenorhabditis elegans rab-3 mutant synapses exhibit impaired function and are partially depleted of vesicles. J Neurosci 1997;**17**(21):8061-73
31. Xuan Z, Manning L, Nelson J, et al. Clarinet (CLA-1), a novel active zone protein required for synaptic vesicle clustering and release. Elife 2017;**6** doi: 10.7554/eLife.29276[published Online First: Epub Date]|.
32. Wu GH, Muthaiyan Shanmugam M, Bhan P, Huang YH, Wagner OI. Identification and Characterization of LIN-2(CASK) as a Regulator of Kinesin-3 UNC-104(KIF1A) Motility and Clustering in Neurons. Traffic 2016;**17**(8):891-907 doi: 10.1111/tra.12413[published Online First: Epub Date]|.
33. Zhen M, Jin Y. The liprin protein SYD-2 regulates the differentiation of presynaptic termini in C. elegans. Nature 1999;**401**(6751):371-5 doi: 10.1038/43886[published Online First: Epub Date]|.
34. Yeh E, Kawano T, Weimer RM, Bessereau JL, Zhen M. Identification of genes involved in synaptogenesis using a fluorescent active zone marker in Caenorhabditis elegans. J Neurosci 2005;**25**(15):3833-41 doi: 10.1523/JNEUROSCI.4978-04.2005[published Online First: Epub Date]|.
35. Ko J, Na M, Kim S, Lee JR, Kim E. Interaction of the ERC family of RIM-binding proteins with the liprin-alpha family of multidomain proteins. J Biol Chem 2003;**278**(43):42377-85 doi: 10.1074/jbc.M307561200[published Online First: Epub Date]|.
36. Chia PH, Patel MR, Wagner OI, Klopfenstein DR, Shen K. Intramolecular regulation of presynaptic scaffold protein SYD-2/liprin-alpha. Mol Cell Neurosci 2013;**56**:76-84 doi: 10.1016/j.mcn.2013.03.004[published Online First: Epub Date]|.
37. Stigloher C, Zhan H, Zhen M, Richmond J, Bessereau JL. The presynaptic dense projection of the Caenorhabditis elegans cholinergic neuromuscular junction localizes synaptic vesicles at the active zone through SYD-2/liprin and UNC-10/RIM-dependent interactions. J Neurosci 2011;**31**(12):4388-96 doi: 10.1523/JNEUROSCI.6164-10.2011[published Online First: Epub Date]|.
38. Kittelmann M, Hegermann J, Goncharov A, et al. Liprin-alpha/SYD-2 determines the size of dense projections in presynaptic active zones in C. elegans. J Cell Biol 2013;**203**(5):849-63 doi: 10.1083/jcb.201302022[published Online First: Epub Date]|.
39. Ackermann F, Waites CL, Garner CC. Presynaptic active zones in invertebrates and vertebrates. EMBO Rep 2015;**16**(8):923-38 doi: 10.15252/embr.201540434[published Online First: Epub Date]|.

40. Shin H, Wyszynski M, Huh KH, et al. Association of the kinesin motor KIF1A with the multimodular protein liprin-alpha. J Biol Chem 2003;**278**(13):11393-401 doi: 10.1074/jbc.M211874200[published Online First: Epub Date]|.
41. Spangler SA, Schmitz SK, Kevenaar JT, et al. Liprin-alpha2 promotes the presynaptic recruitment and turnover of RIM1/CASK to facilitate synaptic transmission. J Cell Biol 2013;**201**(6):915-28 doi: 10.1083/jcb.201301011[published Online First: Epub Date]|.
42. Dai Y, Taru H, Deken SL, et al. SYD-2 Liprin-alpha organizes presynaptic active zone formation through ELKS. Nat Neurosci 2006;**9**(12):1479-87 doi: 10.1038/nn1808[published Online First: Epub Date]|.
43. Ko J, Kim S, Valtschanoff JG, et al. Interaction between liprin-alpha and GIT1 is required for AMPA receptor targeting. J Neurosci 2003;**23**(5):1667-77
44. Goodwin PR, Juo P. The scaffolding protein SYD-2/Liprin-alpha regulates the mobility and polarized distribution of dense-core vesicles in C. elegans motor neurons. PLoS One 2013;**8**(1):e54763 doi: 10.1371/journal.pone.0054763[published Online First: Epub Date]|.
45. Wu YE, Huo L, Maeder CI, Feng W, Shen K. The balance between capture and dissociation of presynaptic proteins controls the spatial distribution of synapses. Neuron 2013;**78**(6):994-1011 doi: 10.1016/j.neuron.2013.04.035[published Online First: Epub Date]|.
46. Edwards SL, Yorks RM, Morrison LM, Hoover CM, Miller KG. Synapse-Assembly Proteins Maintain Synaptic Vesicle Cluster Stability and Regulate Synaptic Vesicle Transport in Caenorhabditis elegans. Genetics 2015;**201**(1):91-116 doi: 10.1534/genetics.115.177337[published Online First: Epub Date]|.
47. Wang Y, Okamoto M, Schmitz F, Hofmann K, Sudhof TC. Rim is a putative Rab3 effector in regulating synaptic-vesicle fusion. Nature 1997;**388**(6642):593-8 doi: 10.1038/41580[published Online First: Epub Date]|.
48. Koushika SP, Richmond JE, Hadwiger G, Weimer RM, Jorgensen EM, Nonet ML. A post-docking role for active zone protein Rim. Nat Neurosci 2001;**4**(10):997-1005 doi: 10.1038/nn732[published Online First: Epub Date]|.
49. Wang Y, Sugita S, Sudhof TC. The RIM/NIM family of neuronal C2 domain proteins. Interactions with Rab3 and a new class of Src homology 3 domain proteins. J Biol Chem 2000;**275**(26):20033-44 doi: 10.1074/jbc.M909008199[published Online First: Epub Date]|.
50. Schoch S, Castillo PE, Jo T, et al. RIM1alpha forms a protein scaffold for regulating neurotransmitter release at the active zone. Nature 2002;**415**(6869):321-6 doi: 10.1038/415321a[published Online First: Epub Date]|.
51. Castillo PE, Schoch S, Schmitz F, Sudhof TC, Malenka RC. RIM1alpha is required for presynaptic long-term potentiation. Nature 2002;**415**(6869):327-30 doi: 10.1038/415327a[published Online First: Epub Date]|.
52. Geppert M, Bolshakov VY, Siegelbaum SA, et al. The role of Rab3A in neurotransmitter release. Nature 1994;**369**(6480):493-7 doi: 10.1038/369493a0[published Online First: Epub Date]|.
53. Johnston PA, Archer BT, 3rd, Robinson K, Mignery GA, Jahn R, Sudhof TC. rab3A attachment to the synaptic vesicle membrane mediated by a conserved polyisoprenylated carboxy-terminal sequence. Neuron 1991;**7**(1):101-9
54. Fischer von Mollard G, Stahl B, Li C, Sudhof TC, Jahn R. Rab proteins in regulated exocytosis. Trends Biochem Sci 1994;**19**(4):164-8
55. Graf ER, Daniels RW, Burgess RW, Schwarz TL, DiAntonio A. Rab3 dynamically controls protein composition at active zones. Neuron 2009;**64**(5):663-77 doi: 10.1016/j.neuron.2009.11.002[published Online First: Epub Date]|.

56. Mahoney TR, Liu Q, Itoh T, et al. Regulation of synaptic transmission by RAB-3 and RAB-27 in Caenorhabditis elegans. Mol Biol Cell 2006;**17**(6):2617-25 doi: 10.1091/mbc.e05-12-1170[published Online First: Epub Date]|.
57. Iwasaki K, Toyonaga R. The Rab3 GDP/GTP exchange factor homolog AEX-3 has a dual function in synaptic transmission. EMBO J 2000;**19**(17):4806-16 doi: 10.1093/emboj/19.17.4806[published Online First: Epub Date]|.
58. Li JY, Jahn R, Dahlstrom A. Rab3a, a small GTP-binding protein, undergoes fast anterograde transport but not retrograde transport in neurons. Eur J Cell Biol 1995;**67**(4):297-307
59. Niwa S, Tanaka Y, Hirokawa N. KIF1Bbeta- and KIF1A-mediated axonal transport of presynaptic regulator Rab3 occurs in a GTP-dependent manner through DENN/MADD. Nat Cell Biol 2008;**10**(11):1269-79 doi: 10.1038/ncb1785[published Online First: Epub Date]|.
60. Nonet ML, Grundahl K, Meyer BJ, Rand JB. Synaptic function is impaired but not eliminated in C. elegans mutants lacking synaptotagmin. Cell 1993;**73**(7):1291-305
61. Nonet ML, Saifee O, Zhao H, Rand JB, Wei L. Synaptic transmission deficits in Caenorhabditis elegans synaptobrevin mutants. J Neurosci 1998;**18**(1):70-80
62. Lemmon MA, Ferguson KM. Molecular determinants in pleckstrin homology domains that allow specific recognition of phosphoinositides. Biochem Soc Trans 2001;**29**(Pt 4):377-84 doi: 10.1042/bst0290377[published Online First: Epub Date]|.
63. Okada Y, Higuchi H, Hirokawa N. Processivity of the single-headed kinesin KIF1A through biased binding to tubulin. Nature 2003;**424**(6948):574-7 doi: 10.1038/nature01804[published Online First: Epub Date]|.
64. Hsu CC, Moncaleano JD, Wagner OI. SUB-CELLULAR DISTRIBUTION OF UNC-104(KIF1A) UPON BINDING TO ADAPTORS AS UNC-16(JIP3), DNC-1(DCTN1/Glued) AND SYD-2(LIPRIN-alpha) IN C. ELEGANS NEURONS. Neuroscience 2011;**176**:39-52 doi: 10.1016/j.neuroscience.2010.12.044[published Online First: Epub Date]|.
65. Campbell RE, Tour O, Palmer AE, et al. A monomeric red fluorescent protein. Proc Natl Acad Sci U S A 2002;**99**(12):7877-82 doi: 10.1073/pnas.082243699[published Online First: Epub Date]|.
66. Zhen M, Jin Y. Presynaptic terminal differentiation: transport and assembly. Curr Opin Neurobiol 2004;**14**(3):280-7 doi: 10.1016/j.conb.2004.05.013[published Online First: Epub Date]|.
67. Taru H, Jin Y. The Liprin homology domain is essential for the homomeric interaction of SYD-2/Liprin-alpha protein in presynaptic assembly. J Neurosci 2011;**31**(45):16261-8 doi: 10.1523/JNEUROSCI.0002-11.2011[published Online First: Epub Date]|.
68. Niwa S, Lipton DM, Morikawa M, et al. Autoinhibition of a Neuronal Kinesin UNC-104/KIF1A Regulates the Size and Density of Synapses. Cell Rep 2016;**16**(8):2129-41 doi: 10.1016/j.celrep.2016.07.043[published Online First: Epub Date]|.
69. Miller KE, DeProto J, Kaufmann N, Patel BN, Duckworth A, Van Vactor D. Direct observation demonstrates that Liprin-alpha is required for trafficking of synaptic vesicles. Curr Biol 2005;**15**(7):684-9 doi: 10.1016/j.cub.2005.02.061[published Online First: Epub Date]|.
70. Gracheva EO, Hadwiger G, Nonet ML, Richmond JE. Direct interactions between C. elegans RAB-3 and Rim provide a mechanism to target vesicles to the presynaptic density. Neurosci Lett 2008;**444**(2):137-42 doi: 10.1016/j.neulet.2008.08.026[published Online First: Epub Date]|.
71. Yogev S, Cooper R, Fetter R, Horowitz M, Shen K. Microtubule Organization Determines Axonal Transport Dynamics. Neuron 2016;**92**(2):449-60 doi: 10.1016/j.neuron.2016.09.036[published Online First: Epub Date]|.
72. Vershinin M, Carter BC, Razafsky DS, King SJ, Gross SP. Multiple-motor based transport and its regulation by Tau. Proc Natl Acad Sci U S A 2007;**104**(1):87-92 doi: 10.1073/pnas.0607919104[published Online First: Epub Date]|.

73. Klopfenstein DR, Tomishige M, Stuurman N, Vale RD. Role of phosphatidylinositol(4,5)bisphosphate organization in membrane transport by the Unc104 kinesin motor. Cell 2002;**109**(3):347-58 doi: 10.1016/s0092-8674(02)00708-0[published Online First: Epub Date]|.
74. Tomishige M, Klopfenstein DR, Vale RD. Conversion of Unc104/KIF1A kinesin into a processive motor after dimerization. Science 2002;**297**(5590):2263-7 doi: 10.1126/science.1073386[published Online First: Epub Date]|.
75. Zheng Q, Ahlawat S, Schaefer A, Mahoney T, Koushika SP, Nonet ML. The vesicle protein SAM-4 regulates the processivity of synaptic vesicle transport. PLoS Genet 2014;**10**(10):e1004644 doi: 10.1371/journal.pgen.1004644[published Online First: Epub Date]|.
76. Tyers M, Haslam RJ, Rachubinski RA, Harley CB. Molecular analysis of pleckstrin: the major protein kinase C substrate of platelets. J Cell Biochem 1989;**40**(2):133-45 doi: 10.1002/jcb.240400202[published Online First: Epub Date]|.
77. Haslam RJ, Koide HB, Hemmings BA. Pleckstrin domain homology. Nature 1993;**363**(6427):309-10 doi: 10.1038/363309b0[published Online First: Epub Date]|.
78. Shaw G. The pleckstrin homology domain: an intriguing multifunctional protein module. Bioessays 1996;**18**(1):35-46 doi: 10.1002/bies.950180109[published Online First: Epub Date]|.
79. Musacchio A, Gibson T, Rice P, Thompson J, Saraste M. The PH domain: a common piece in the structural patchwork of signalling proteins. Trends Biochem Sci 1993;**18**(9):343-8
80. Gibson TJ, Hyvonen M, Musacchio A, Saraste M, Birney E. PH domain: the first anniversary. Trends Biochem Sci 1994;**19**(9):349-53
81. M AL, M F, J S, K F. Regulatory recruitment of signalling molecules to the cell membrane by pleckstrinhomology domains. Trends Cell Biol 1997;**7**(6):237-42 doi: 10.1016/S0962-8924(97)01065-9[published Online First: Epub Date]|.
82. Kavran JM, Klein DE, Lee A, et al. Specificity and promiscuity in phosphoinositide binding by pleckstrin homology domains. J Biol Chem 1998;**273**(46):30497-508
83. Richens JL, Lane JS, Bramble JP, O'Shea P. The electrical interplay between proteins and lipids in membranes. Biochim Biophys Acta 2015;**1848**(9):1828-36 doi: 10.1016/j.bbamem.2015.03.017[published Online First: Epub Date]|.
84. Ward S, Burke DJ, Sulston JE, et al. Genomic organization of major sperm protein genes and pseudogenes in the nematode Caenorhabditis elegans. Journal of molecular biology 1988;**199**(1):1-13
85. Schneider CA, Rasband WS, Eliceiri KW. NIH Image to ImageJ: 25 years of image analysis. Nature methods 2012;**9**(7):671-5
86. Brenner S. The genetics of Caenorhabditis elegans. Genetics 1974;**77**(1):71-94
87. Kumar J, Choudhary BC, Metpally R, et al. The Caenorhabditis elegans Kinesin-3 motor UNC-104/KIF1A is degraded upon loss of specific binding to cargo. PLoS Genet 2010;**6**(11):e1001200 doi: 10.1371/journal.pgen.1001200[published Online First: Epub Date]|.
88. Li Q, Lau A, Morris TJ, Guo L, Fordyce CB, Stanley EF. A syntaxin 1, Galpha(o), and N-type calcium channel complex at a presynaptic nerve terminal: analysis by quantitative immunocolocalization. J Neurosci 2004;**24**(16):4070-81 doi: 10.1523/JNEUROSCI.0346-04.2004[published Online First: Epub Date]|.

FIGURE LEGENDS

Figure 1: SYD-2 mRNA expression level by Real-Time PCR analysis and UNC-104/SYD-2 protein-protein interactions by SDS-PAGE and Co-IP assay. (A) Plot indicating relative SYD-2 expression level in UNC-10 mutants. Keeping the wild-type as reference point, *e102* allele displays increased expression by 1.58 fold and *md1117* allele shows increase by 1.37 fold respectively. (B) Expression level of SYD-2 decreases by 50% in *rab-3(js49)* mutant's. The RNA levels were normalized to *cdc-42* (internal control). (C) % SYD-2 signal intensity (quantified from lysate section in 1E) in *unc-10(md1117; e102)* mutants. (D) % SYD-2 signal intensity in *rab-3(js49)* mutant (quantified from lysate section in 1G). (E) Western blot and Co-IP assays using lysates from worms expressing UNC-104::GFP in wild-type and different UNC-10 mutant alleles *(e102 and md1117).* Co-IP assays are standardized by amounts of detected IgG. (F) %SYD-2 signal intensity in each sample is normalized against IgG in the respective UNC-104 sample. (G) Shows Western blot and Co-IP bands in lysates from worms expressing UNC-104::mRFP in wild-type and *rab-3(js49)* mutants. (H) %SYD-2 signal intensity in each sample is normalized against IgG. (For antibody details, refer to the Methods and Materials section)P-values: *P<0.05, **P<0.01, ***P<0.001, ****P<0.0001 (Student's t-test). Error bar: ± SEM. No of trials: 3.

Figure 2: UNC-104/SYD-2 interaction (using colocalization analysis and BiFC) in the absence of UNC-10 and RAB-3. (A) UNC-104 and SYD-2 colocalization in the nerve ring of wild-type, *unc-10(md1117)*, *rab-3(js49)* single mutants and *unc-10(md1117);rab-3(js49)* double mutants. (B) Quantification of colocalization from images shown in (A) (N=20). White arrows indicate specific colocalization occurrences. (C) UNC-104 and SYD-2 BiFC signals in the nerve ring of wild-type, *unc-10(md1117)* and *rab-3(js49)* mutants respectively. UNC-104/UNC-104 BiFC represents positive control and UNC-104/empty BiFC represents negative control. White

dashed lines indicate the border of the worm. (D) Quantification of fluorescence intensity from images shown in (C) (N=25). A-anterior and P-posterior direction. P-values: *P<0.05, **P<0.01, ***P<0.001, ****P<0.0001 (Student's t-test). Error bar: ± SEM. Scale bar: 10 µm.

Figure 3: Effect of active zone proteins SYD-2/UNC-10/RAB-3 on axonal UNC-104 clustering in sublateral and ALM neurons. (A) UNC-104 axonal clustering in *syd-2, unc-10* and *rab-3* mutants as observed in sublateral neurons. (B) Cluster size (area) quantification from (A). (C) Stacks of the ALM neuron after digital straightening reflecting characteristic UNC-104 clustering in wild-type, *syd-2(ok217), unc-10(md1117)* and *rab-3(js49)* mutants' respectively. (D) Quantification of average distances travelled from the axonal hillock to distal areas in the neuron (data taken from (C)). (E) Cluster size (area) quantification from (C). P-values: *P<0.05, **P<0.01, ***P<0.001, ****P<0.0001 (Student's t-test). Error bar: ± SEM. N= 20. Scale bar: 10 µm.

Figure 4: Single/Double mutant analysis to investigate the effects on UNC-104 motility. (A) Anterograde velocity of UNC-104 in wild-type, in worms with either *syd-2, unc-10, rab-3* knockouts as well as combination of these with RNAi knockdown, overexpression and double mutants respectively. (B) Anterograde run length of observed UNC-104 particles. White wild cards indicates the T-tests between *unc-10(md1117) and unc-10(md1117);rab-3(js49)* double mutants. (C) Anterograde moving persistency of UNC-104 particles. (D) Effect on UNC-104's pausing behavior. White wild cards "*" indicates the T-tests between *unc-10(md1117) and unc-10(md1117);rab-3(js49)* double mutant. Analyzed total moving events: UNC-104(wt)=689, *syd-2(ok217)*= 535, *unc-10(md1117)*= 515, *rab-3(js49)*= 520, *unc-10;rab-3* double mutant= 522, *syd-2(ok217);unc-10 RNAi*= 536, r*ab-3(js49);syd-2 RNAi*= 518, *rab-3 rescue* = 535, *syd-2 rescue* = 323, *unc-10 rescue* = 495, *syd-2 overexpression* = 595, *syd-2 overexpression;unc-10 RNAi*= 570. P-values: *P<0.05, **P<0.01, ***P<0.001, ****P<0.0001 (Student's t-test). Error bar: ± SEM.

Figure 5: Effect of UNC-10 and SYD-2 on synaptic vesicle trafficking and cargo accumulation. (A) Anterograde velocity of SNB-1 in wild-type worms, *syd-2* and *unc-10* mutant worms and *rab-3* RNAi background. Similarly, (B) represents the anterograde velocity of RAB-3 containing vesicles in wild-type worms, *syd-2* and *unc-10* mutants' and *snb-1* RNAi background. (C) Anterograde run length travelled by SNB-1 while (D) represents the anterograde run length travelled by RAB-3 containing vesicles respectively. (E) Images of ALM neurons digitally straightened and stacked reflecting SNB-1 clustering in wild-type, *syd-2* and *unc-10* mutant worms. (F) Quantification of the average distance travelled by SNB-1 from axonal hillocks (data taken from images as shown in (E)) (N=20). Likewise, (G) represents the images of ALM neurons digitally straightened and stacked reflecting RAB-3 clustering in wild-type, *syd-2* and *unc-10* mutant worms. (H) Shows quantification of average distance from (G) (N=20). Analyzed total moving events: SNB-1(wt)= 510, *Rab-3 RNAi*= 360, *syd-2(ok217)*= 439, *unc-10(md1117)*= 518, RAB-3(wt)= 513, *snb-1 RNAi*=306, *syd-2(ok217)*= 508, *unc-10(md1117)*= 509. P-values: *P<0.05, **P<0.01, ***P<0.001, ****P<0.0001 (Student's t-test). Error bar: ± SEM. Scale bar: 10 µm.

Figure 6: Interaction between RAB-3/UNC-104 and SNB-1/UNC-104 in the presence or absence of the motor's PH domain. (A) Shows RAB-3 colocalization with full length UNC-104. (B) Shows RAB-3 colocalization with UNC-104 with a deleted PH domain. (C) Colocalization of UNC-104 and RAB-3 in *syd-2* and *unc-10* mutant background. (D) Quantification of UNC-104/RAB-3 colocalization from images shown in (A, B and C). (E) Shows SNB-1 colocalization with full length UNC-104 in wild type and *unc-10* mutant and in UNC-104 with a deleted PH domain. (F) Quantification of UNC-104/SNB-1 colocalization from images shown in panel (E). (G-H) Colocalization of UNC-104ΔPH/RAB-3 and UNC-104ΔPH/SNB-1 in dorsal and ventral

cord neurons. P-values: *P<0.05, **P<0.01, ***P<0.001, ****P<0.0001 (Student's t-test). Error bar: ± SEM. N=20. Scale bar: 10 µm.

Figure 7: Model depicting the role of UNC-10/RAB-3 on stabilizing the interaction of UNC-104 and SYD-2 affecting synaptic vesicle transport. (A) The interaction between UNC-104's PH domain and the lipid-containing vesicle membrane. (B) Loss of UNC-10 and RAB-3 results in loss of SYD-2 and UNC-104 interaction in turn leading to measurable reduction in UNC-104's motility. Interestingly, the absence of UNC-10 and SYD-2 also affects the binding of UNC-104 to RAB-3 containing vesicles. The importance of SYD-2 and UNC-10 lies in its scaffolding function where they regulate motor organization and cargo binding. (C) Presence of a hypothetical linker that may act as an important stabilizer, especially considering the notion that the cargo is multiple size of the motor and pushing itself through the crowded axoplasm.

FIGURES

FIGURE 1

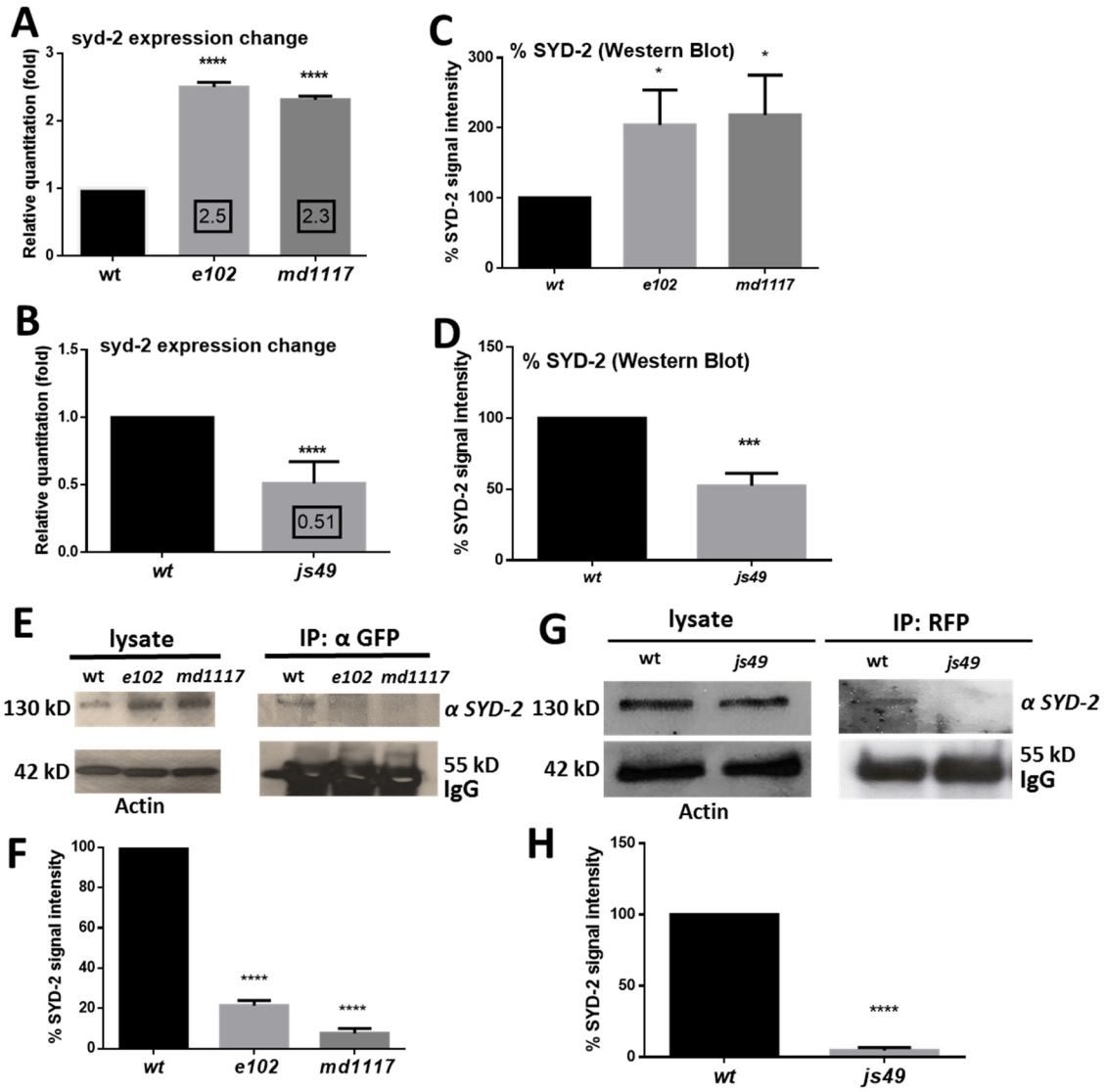

FIGURE 2

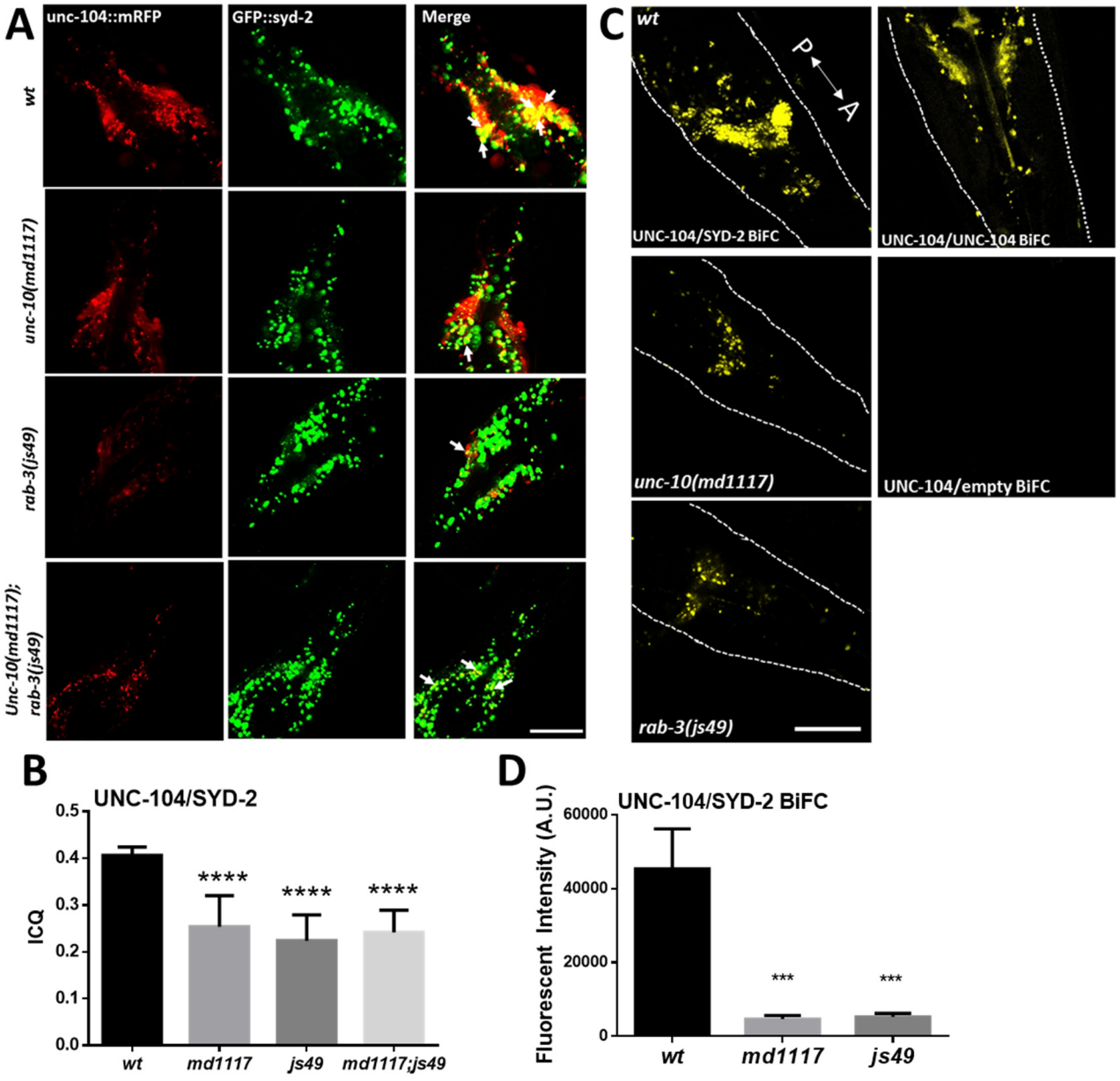
A
unc-104::mRFP
GFP::syd-2
Merge
wt
unc-10(md1117)
rab-3(js49)
Unc-10(md1117); rab-3(js49)
C
wt
P
A
UNC-104/SYD-2 BiFC
UNC-104/UNC-104 BiFC
unc-10(md1117)
UNC-104/empty BiFC
rab-3(js49)
B
UNC-104/SYD-2
ICQ
0.5
0.4
0.3
0.2
0.1
0.0
****
****
****
wt
md1117
js49
md1117;js49
D
UNC-104/SYD-2 BiFC
Fluorescent Intensity (A.U.)
60000
40000
20000
0
***
***
wt
md1117
js49

FIGURE 3

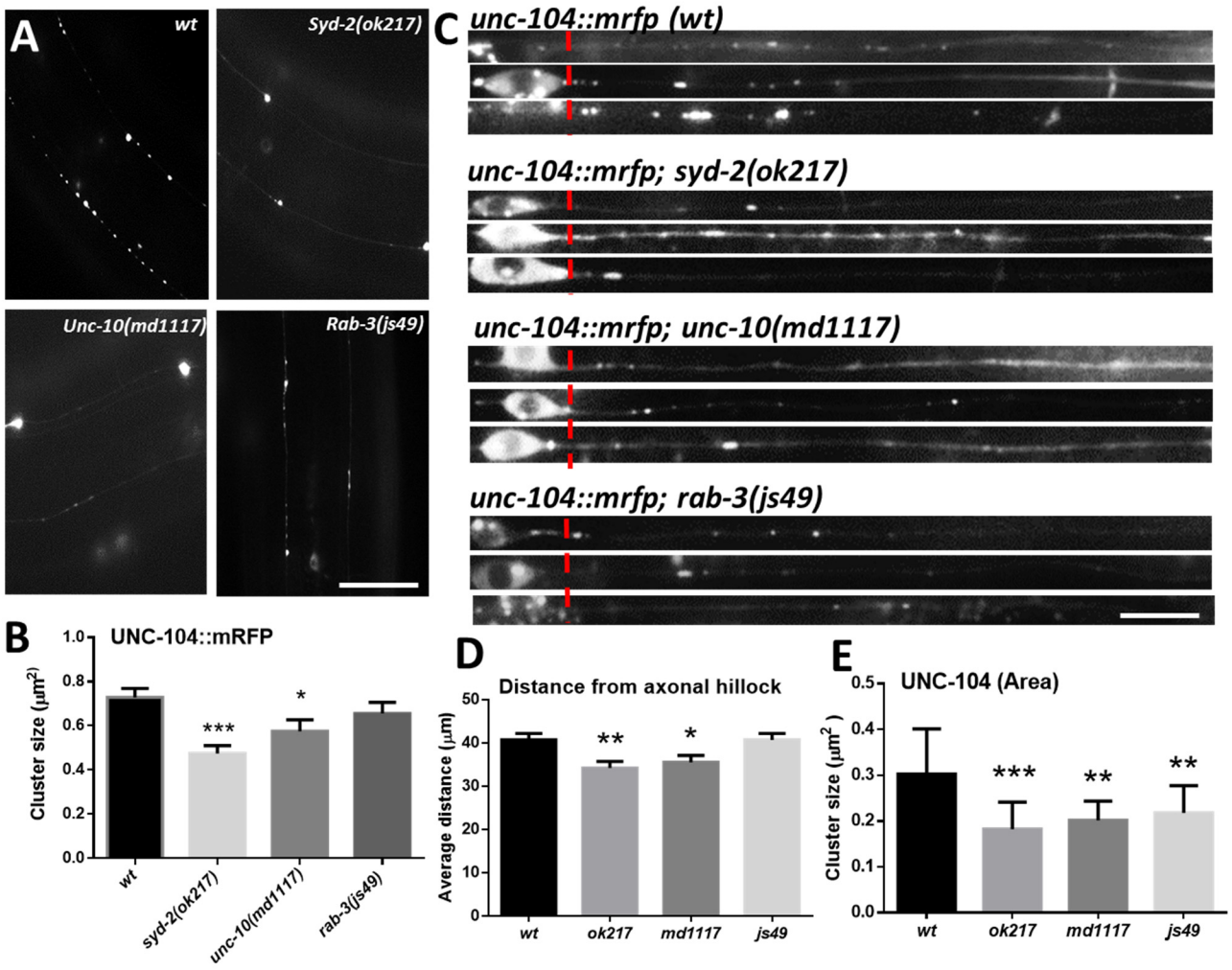
A
wt
Syd-2(ok217)
Unc-10(md1117)
Rab-3(js49)
C
unc-104::mrfp (wt)
unc-104::mrfp; syd-2(ok217)
unc-104::mrfp; unc-10(md1117)
unc-104::mrfp; rab-3(js49)
B
UNC-104::mRFP
Cluster size (μm²)
1.0
0.8
0.6
0.4
0.2
0.0
***
*
wt
syd-2(ok217)
unc-10(md1117)
rab-3(js49)
D
Distance from axonal hillock
Average distance (μm)
50
40
30
20
10
0
**
*
wt
ok217
md1117
js49
E
UNC-104 (Area)
Cluster size (μm²)
0.5
0.4
0.3
0.2
0.1
0.0
***
**
**
wt
ok217
md1117
js49

FIGURE 4

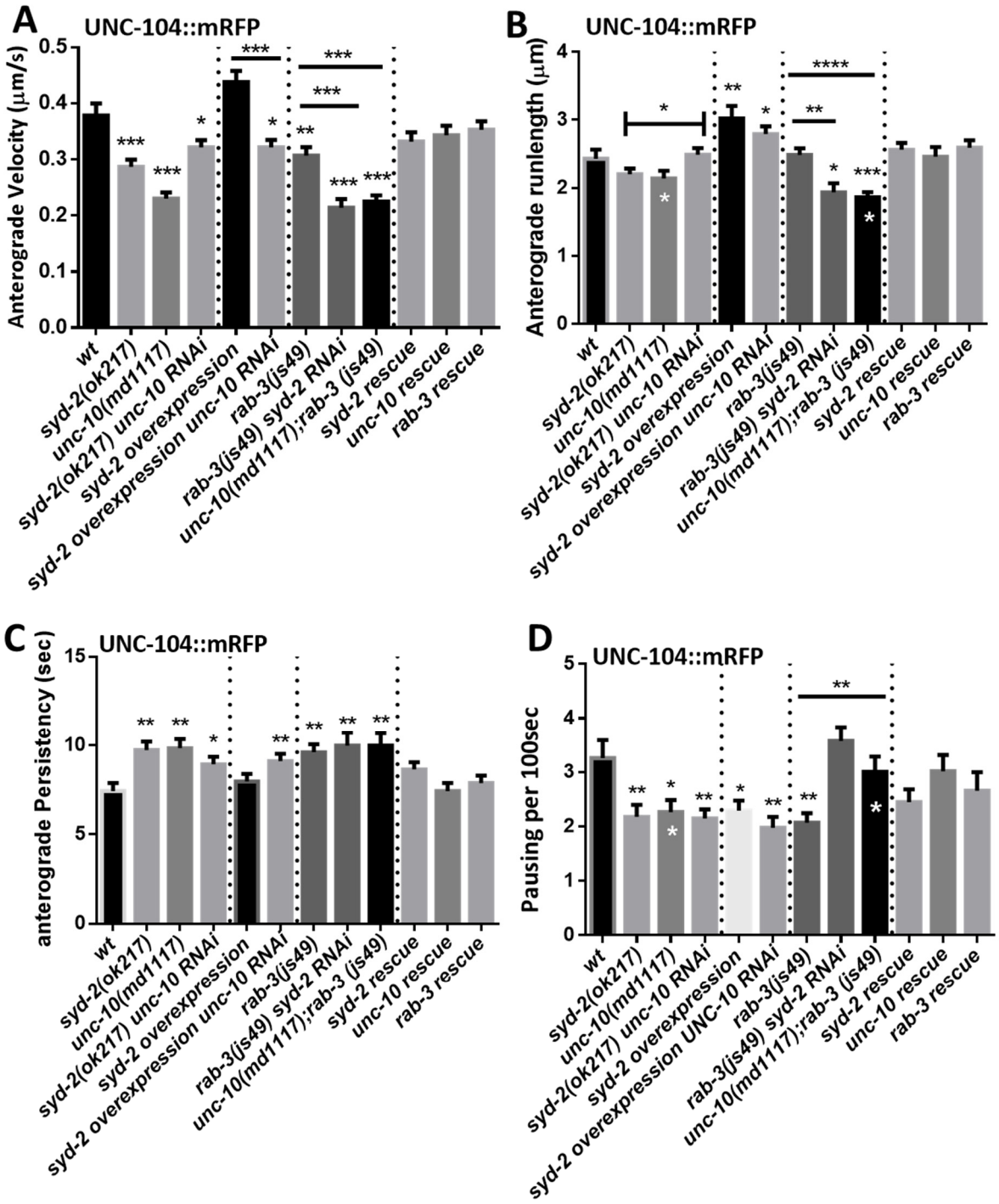
A
UNC-104::mRFP
Anterograde Velocity (μm/s)
0.0
0.1
0.2
0.3
0.4
0.5
wt
syd-2(ok217)
unc-10(md1117)
syd-2(ok217) unc-10 RNAi
syd-2 overexpression
syd-2 overexpression unc-10 RNAi
rab-3(js49)
rab-3(js49) syd-2 RNAi
unc-10(md1117);rab-3 (js49)
syd-2 rescue
unc-10 rescue
rab-3 rescue
B
UNC-104::mRFP
Anterograde runlength (μm)
0
1
2
3
4
C
UNC-104::mRFP
anterograde Persistency (sec)
0
5
10
15
D
UNC-104::mRFP
Pausing per 100sec
0
1
2
3
4
5
syd-2 overexpression UNC-10 RNAi

FIGURE 5

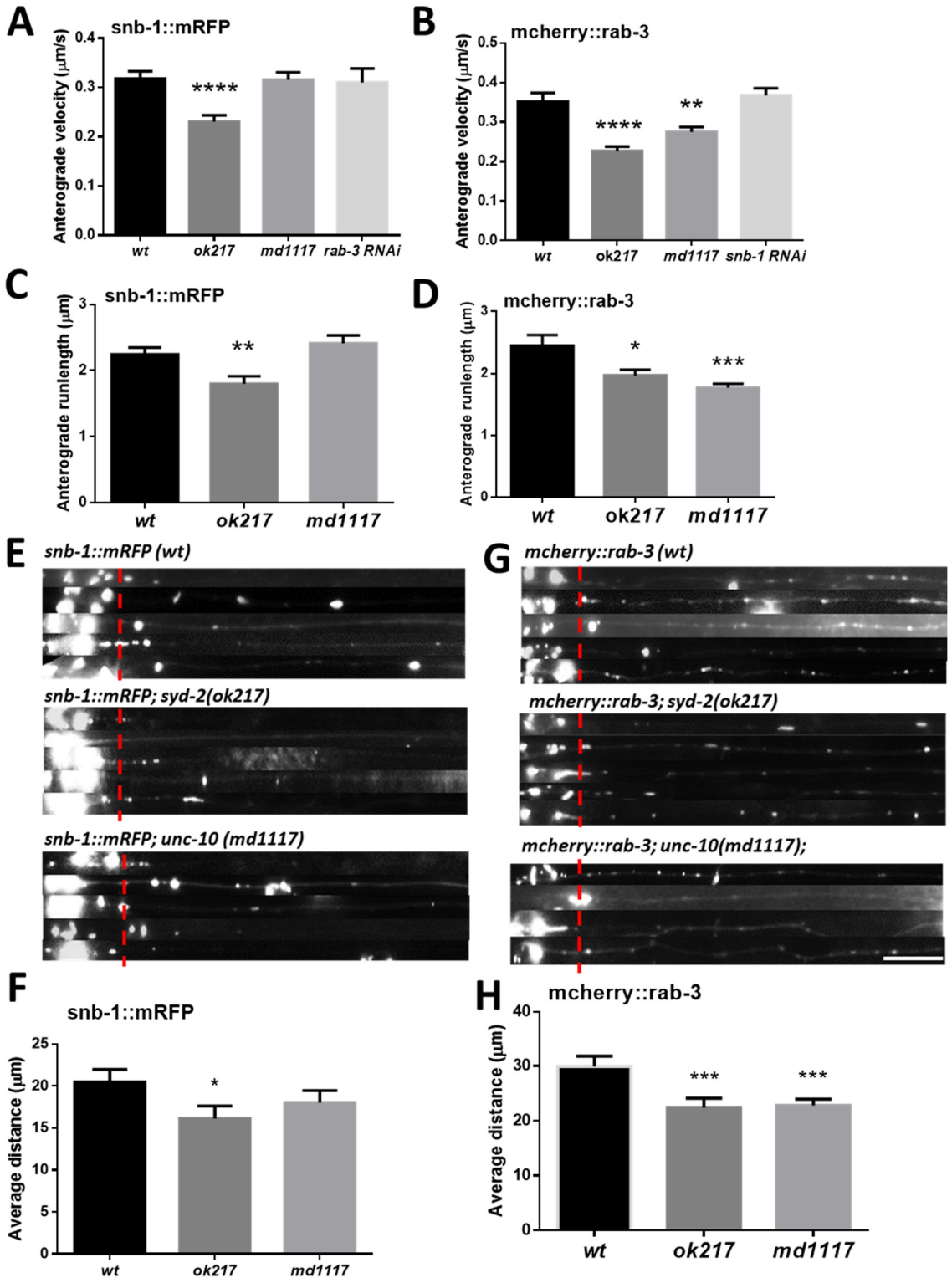
A
snb-1::mRFP
Anterograde velocity (μm/s)
0.4
0.3
0.2
0.1
0.0
****
wt
ok217
md1117
rab-3 RNAi
B
mcherry::rab-3
Anterograde velocity (μm/s)
0.5
0.4
0.3
0.2
0.1
0.0
****
**
wt
ok217
md1117
snb-1 RNAi
C
snb-1::mRFP
Anterograde runlength (μm)
3
2
1
0
**
wt
ok217
md1117
D
mcherry::rab-3
Anterograde runlength (μm)
3
2
1
0
*
***
wt
ok217
md1117
E
snb-1::mRFP (wt)
snb-1::mRFP; syd-2(ok217)
snb-1::mRFP; unc-10 (md1117)
G
mcherry::rab-3 (wt)
mcherry::rab-3; syd-2(ok217)
mcherry::rab-3; unc-10(md1117);
F
snb-1::mRFP
Average distance (μm)
25
20
15
10
5
0
*
wt
ok217
md1117
H
mcherry::rab-3
Average distance (μm)
40
30
20
10
0
***
***
wt
ok217
md1117

FIGURE 6

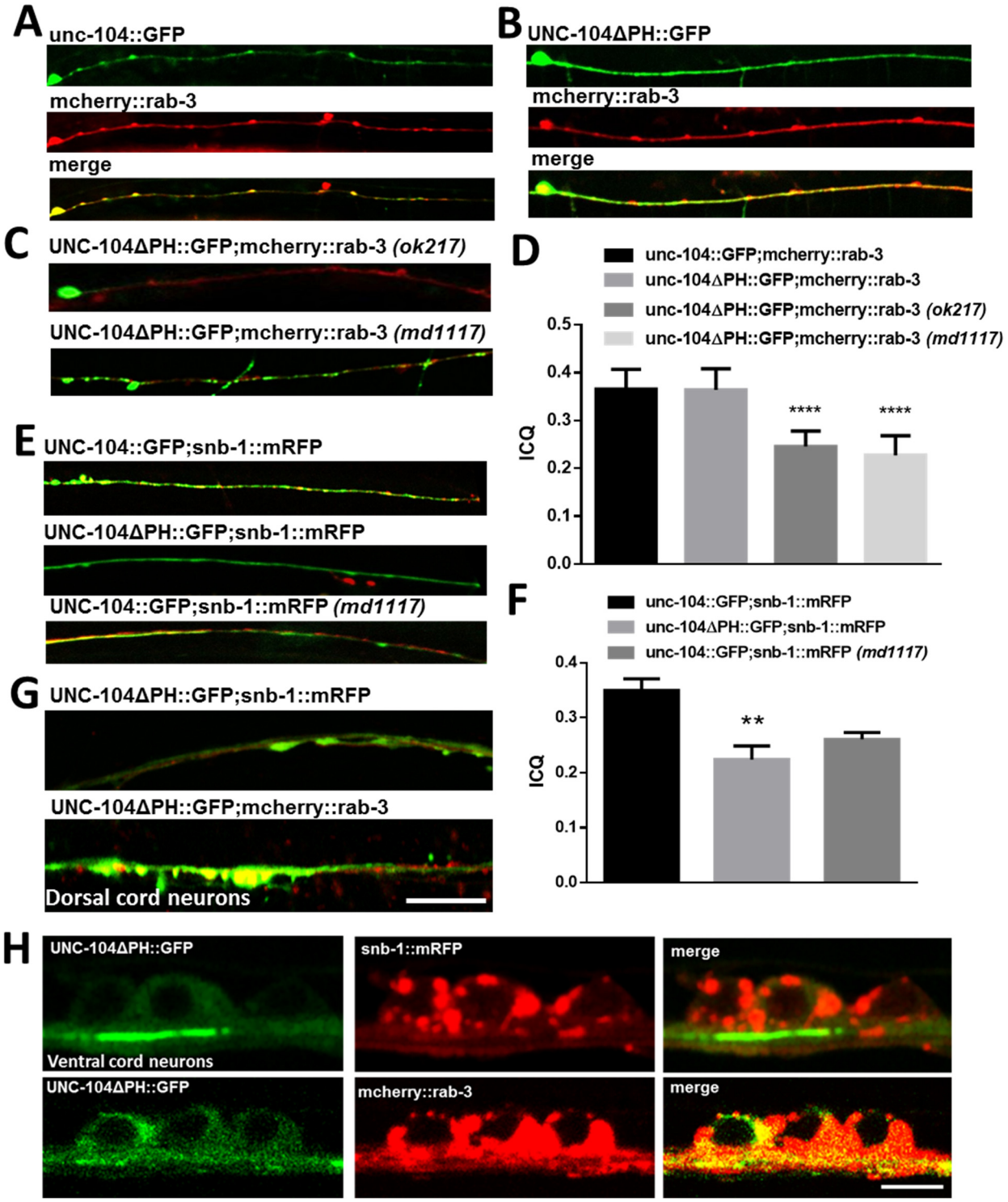
A
unc-104::GFP
mcherry::rab-3
merge
B
UNC-104ΔPH::GFP
mcherry::rab-3
merge
C
UNC-104ΔPH::GFP;mcherry::rab-3 (ok217)
UNC-104ΔPH::GFP;mcherry::rab-3 (md1117)
D
unc-104::GFP;mcherry::rab-3
unc-104ΔPH::GFP;mcherry::rab-3
unc-104ΔPH::GFP;mcherry::rab-3 (ok217)
unc-104ΔPH::GFP;mcherry::rab-3 (md1117)
ICQ
0.5
0.4
0.3
0.2
0.1
0.0
****
****
E
UNC-104::GFP;snb-1::mRFP
UNC-104ΔPH::GFP;snb-1::mRFP
UNC-104::GFP;snb-1::mRFP (md1117)
F
unc-104::GFP;snb-1::mRFP
unc-104ΔPH::GFP;snb-1::mRFP
unc-104::GFP;snb-1::mRFP (md1117)
ICQ
0.4
0.3
0.2
0.1
0.0
**
G
UNC-104ΔPH::GFP;snb-1::mRFP
UNC-104ΔPH::GFP;mcherry::rab-3
Dorsal cord neurons
H
UNC-104ΔPH::GFP
snb-1::mRFP
merge
Ventral cord neurons
UNC-104ΔPH::GFP
mcherry::rab-3
merge

FIGURE 7

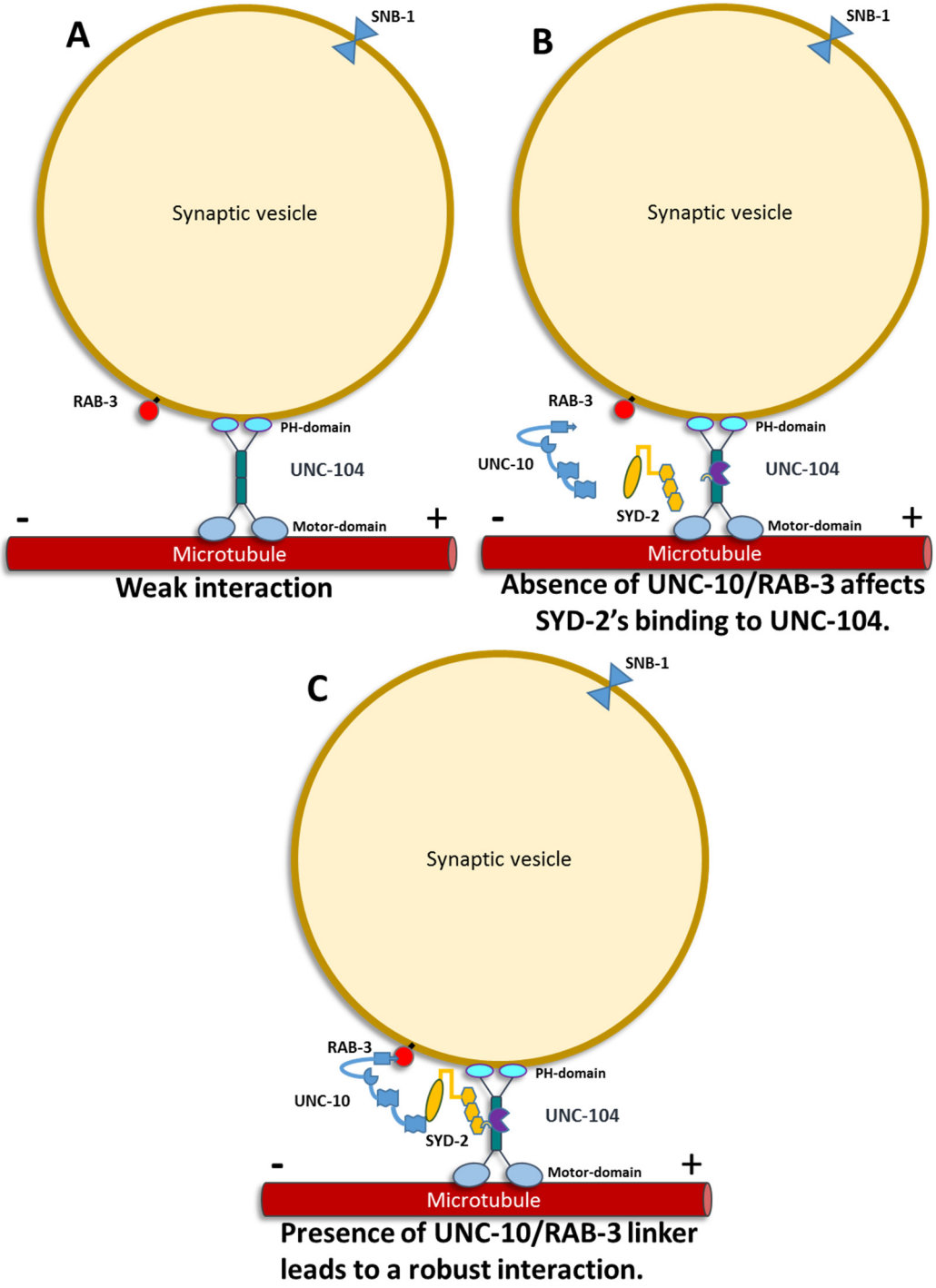
A
SNB-1
Synaptic vesicle
RAB-3
PH-domain
UNC-104
-
Motor-domain
+
Microtubule
Weak interaction
B
SNB-1
Synaptic vesicle
RAB-3
PH-domain
UNC-10
UNC-104
SYD-2
-
Motor-domain
+
Microtubule
Absence of UNC-10/RAB-3 affects SYD-2's binding to UNC-104.
C
SNB-1
Synaptic vesicle
RAB-3
PH-domain
UNC-10
UNC-104
SYD-2
-
Motor-domain
+
Microtubule
Presence of UNC-10/RAB-3 linker leads to a robust interaction.

SUPPLEMENTARY MATERIAL

SUPPLEMENTARY FIGURE LEGENDS

Suppl. Figure S1: (A) Diagrammatic representation of the domain structures of UNC-104, UNC-10, SYD-2 and RAB-3 respectively. Mutant alleles are marked in red. (B) Schematic diagram of a neuron with blue double sided arrows indicating the distances travelled from the axonal hillock to farther distal regions. (C) RAB-3 and SNB-1 BiFC signals in the somas of amphid neurons that also colocalizes with UNC-104. Scale bar: 10 µm.

Suppl. Figure S2: (A) The line scan displays two colored peaks each representing UNC-104 and RAB-3. Overlapping regions of these peaks further show sites of UNC-104 and RAB-3 colocalization. (B) The line scan displays two colored peaks each representing UNC-104 with a deleted PH domain and RAB-3. (C-D) This line scan represents the colocalization between UNC-104 with a deleted PH domain and RAB-3 in the absence of SYD-2 and UNC-10 respectively.

Suppl. Figure S3: (A) The line scan displays two colored peaks each representing UNC-104 and SNB-1. Overlapping regions of these peaks further show sites of UNC-104 and SNB-1 colocalization. (B) The line scan displays two colored peaks each representing UNC-104 with a deleted PH domain and SNB-1. (C) This line scan represents the colocalization between UNC-104 and SNB-1 in the absence of UNC-10.

SUPPLEMENTARY FIGURES

SUPPLEMENTARY FIGURE S1

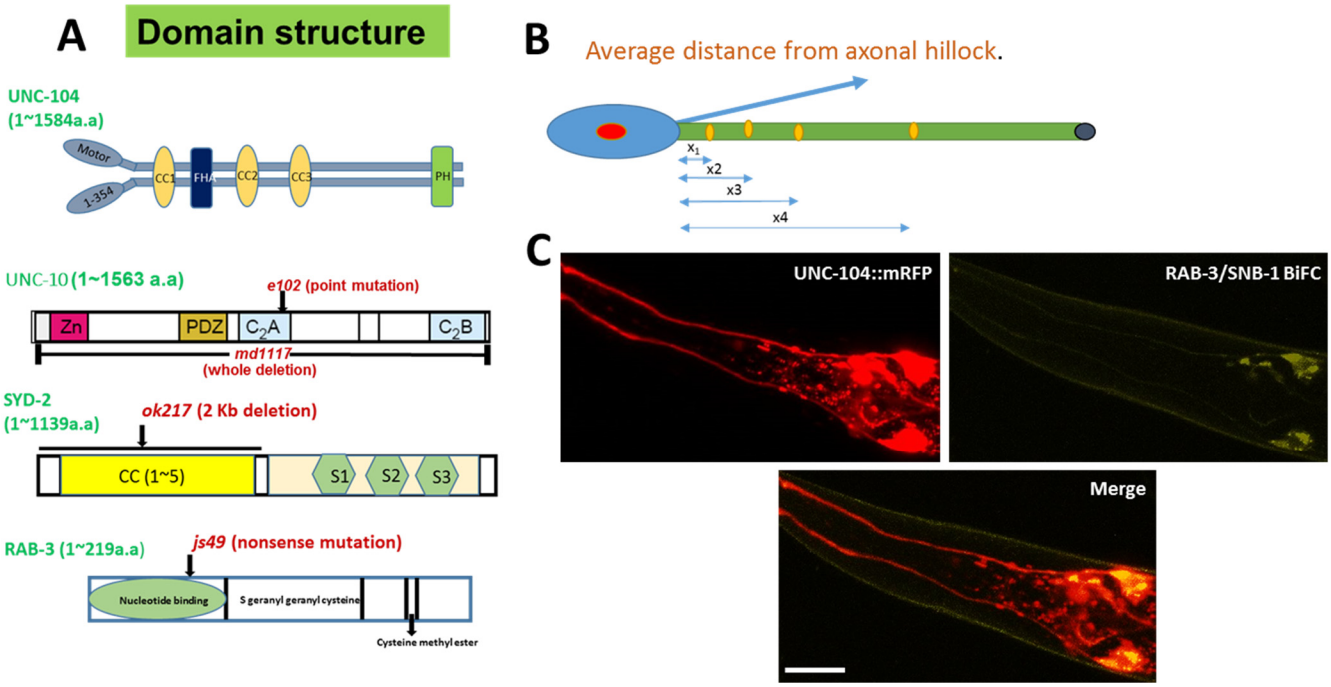

SUPPLEMENTARY FIGURE S2

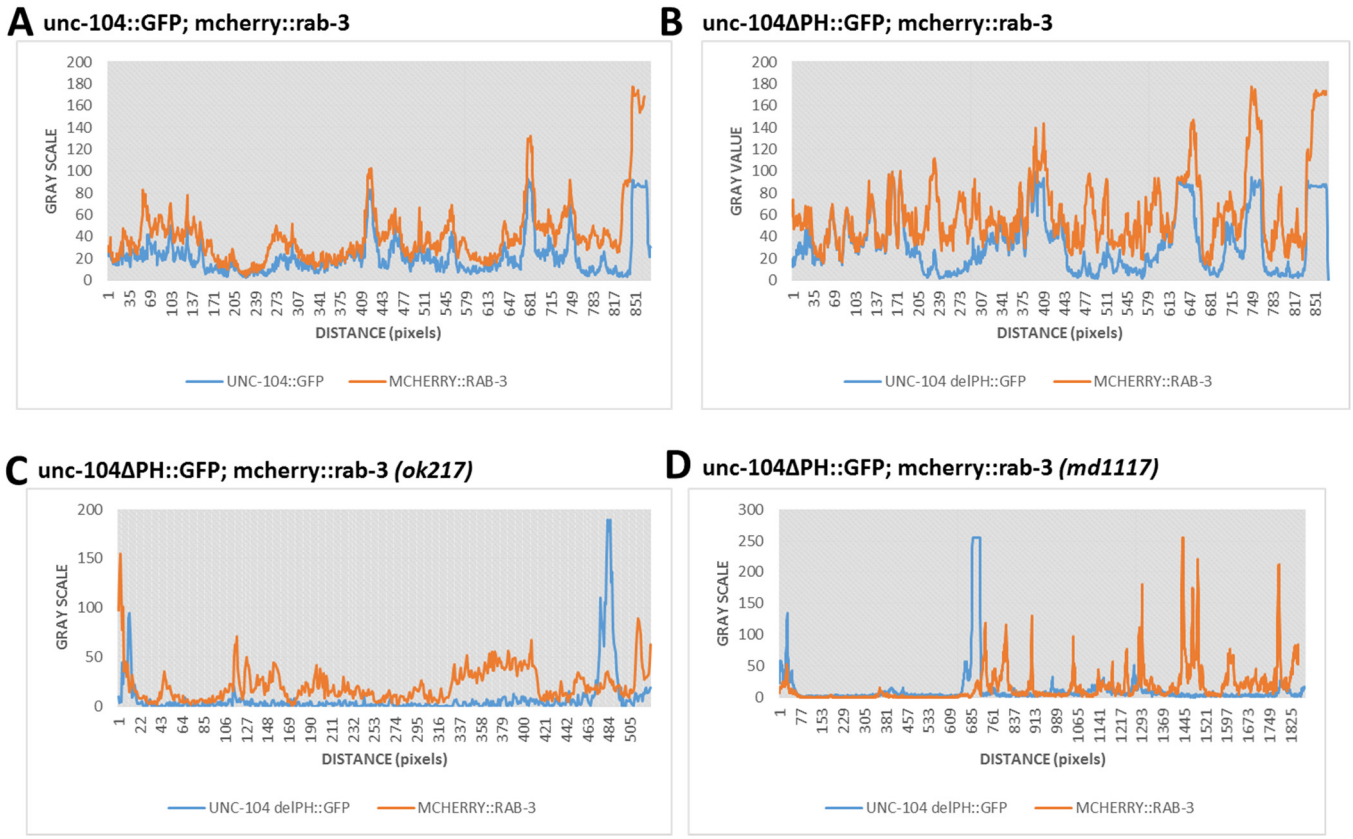

SUPPLEMENTARY FIGURE S3

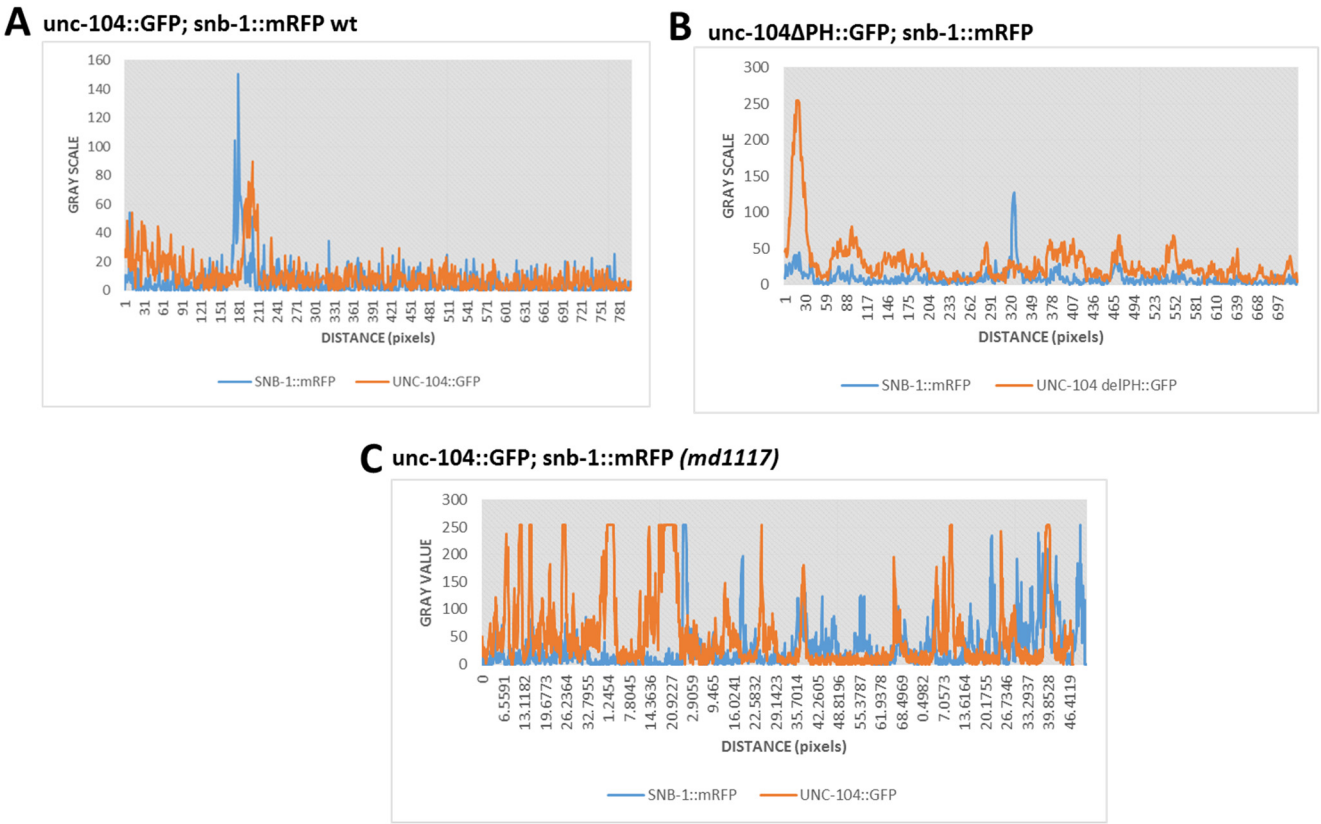

SUPPLEMENTARY TABLE LEGENDS

Supplementary Table S1: Accompanying table with details to Figure 3B.

Supplementary Table S2: Accompanying table with details to Figure 3D+E.

Supplementary Table S3: Accompanying table with details to Figure 4A+B.

Supplementary Table S4: Accompanying table with details to Figure 4C+D.

Supplementary Table S5: Accompanying table with details to Figure 5A-D.

Supplementary Table S6: Accompanying table with details to Figure 5F+H.

SUPPLEMENTARY TABLES

Suppl. Table S1

unc-104 ::mRFP	*wt*	*syd-2 (ok217)*	*unc-10 (md1117)*	*rab-3 (js49)*
Average cluster size(μM^2)	**0.72±0.64**	**0.474±0.38**	**0.574±0.48**	**0.655±0.56**
Total neurite length (mm)	1.95	2.44	1.44	1.28
Cluster per 100µm	19.55	15.5	22.7	25.4
# cluster	382	380	330	326

Suppl. Table S2

unc-104::mRFP	*wt*	*syd-2(ok217)*	*unc-10(md1117)*	*rab-3(js49)*
Average distance	40.77±1.510	34.26±1.563	35.60±1.602	39.7±1.52
Cluster size (μm^2)	0.302±0.098	0.182±0.058	0.202±0.041	0.218±0.059

Suppl. Table S3

	Anterograde Velocity (µm/s)			Anterograde runlength (µm)	
unc-104::mRFP	Mean	SEM	N	Mean	SEM
wt	0.378	0.021	165	2.430	0.137
syd-2(ok217)	0.280	0.012	193	2.203	0.082
unc-10(md1117)	0.230	0.010	155	2.139	0.113
rab-3(js49)	0.306	0.015	194	2.483	0.098
syd-2(ok217)unc-10 RNAi	0.321	0.012	223	2.487	0.098
rab-3(js49)syd-2 RNAi	0.214	0.015	170	1.936	0.130
rab-3(js49);unc-10(md1117)	0.224	0.011	172	1.863	0.076
syd-2 rescue	0.331	0.016	175	2.563	0.099
unc-10 rescue	0.348	0.017	159	2.460	0.141
rab-3 rescue	0.353	0.015	202	2.590	0.110

Suppl. Table S4

	Anterograde persistency (sec)		Pausing per 100 sec	
unc-104::mRFP	Mean	SEM	Mean	SEM
wt	7.425	0.459	3.257	0.333
syd-2(ok217)	9.727	0.484	2.179	0.220
unc-10(md1117)	9.830	0.521	2.264	0.220
rab-3(js49)	9.607	0.448	2.067	0.175
syd-2(ok217)unc-10 RNAi	8.925	0.430	2.150	0.165
rab-3(js49)syd-2 RNAi	9.982	0.727	3.570	0.263
rab-3(js49);unc-10(md1117)	9.982	0.693	3.008	0.279
syd-2 rescue	8.642	0.402	2.449	0.231
unc-10 rescue	7.411	0.450	3.014	0.301
rab-3 rescue	7.886	0.412	2.658	0..339

Suppl. Table S5

	Anterograde Velocity (µm/s)			Anterograde runlength (µm)	
snb-1::mRFP	Mean	SEM	N	Mean	SEM
wt	0.317	0.015	158	2.243	0.106
syd-2(ok217)	0.230	0.012	159	1.798	0.115
unc-10(md1117)	0.315	0.014	203	2.411	0.123
Rab-3 RNAi	0.3104	0.028	149		
mcherry::rab-3					
wt	0.351	0.021	174	2.451	0.170
syd-2(ok217)	0.226	0.011	158	1.970	0.092
unc-10(md1117)	0.275	0.012	182	1.768	0.064
Snb-1 RNAi	0.367	0.018	184		

Suppl. Table S6

	snb-1::mRFP	mcherry::rab-3
	Average distance (µm)	Average distance (µm)
wt	20.49±1.503	29.93±1.839
syd-2(ok217)	16.13±1.507	22.41±1.706
unc-10(md1117)	18.03±1.431	22.81±1.142